

ENGINEERING EXPERIMENT STATION
of the Georgia Institute of Technology
Atlanta, Georgia

22
128

FINAL REPORT

PROJECT NO. B-220

PARTICLE CLASSIFIER EMPLOYING ADHESION PRINCIPLE

By

JOHN H. BURSON, KOICHI IINOYA, CLYDE ORR, JR.

COVERING THE PERIOD
SEPTEMBER 1, 1960 through AUGUST 31, 1962

RESEARCH GRANT NO. AP-120 (C1)

Prepared for

DIVISION OF AIR POLLUTION
BUREAU OF STATE SERVICES
DEPARTMENT OF HEALTH, EDUCATION, AND WELFARE
WASHINGTON 25, D.C.

TABLE OF CONTENTS

	Page
I. SUMMARY	1
II. INTRODUCTION.	3
III. THEORETICAL STUDIES OF PARTICLE MECHANICS	5
A. General Considerations.	5
B. Theory of Adhesion between a Sphere and a Plane Surface Due to a Liquid Film.	6
C. Calculation of Adhesive Forces Due to a Liquid Film between Particles and Surfaces.	8
1. A Sphere and a Plane Surface.	9
2. Between Two Spheres	11
D. Calculation of Limiting Particle Sizes for Adhesion to Horizontal and Vertical Plane Surfaces.	15
1. Horizontal Surfaces	15
2. Vertical Surfaces	18
E. Calculation of the Classifying Effect Arising from the Trajectories of Bounced Particles	20
F. Calculation of the Drag Force Required to Remove Small Adhered Particles from Surfaces	22
G. Calculation of the Theoretical Cross-Section Profiles of Liquid Pools between Particles and Surfaces.	27
1. A Sphere and a Plane Surface, or Two Spheres.	27
2. A Vertical Plane, or a Cylinder, and a Horizontal Liquid Surface.. . . .	30
IV. EXPERIMENTAL TECHNIQUES AND RESULTS	37
A. General Procedure	37
B. Types of Apparatus.	37
1. Flexible Belt Designs	37
a. Method I.	37

TABLE OF CONTENTS (CONTINUED)

	Page
b. Method II	38
c. Method III.	38
d. Method IV	40
2. Rotating and Stationary Cylinder Designs.	40
3. Rotating Disk Designs	41
4. System Components	43
a. Vibrating Devices	43
b. Wiping Devices.	43
c. Substrate Materials	46
d. Air Jet Assembly.	46
e. Power Feed Systems.	48
(1) Feed Jet	48
(2) Vacuum Feed Enclosure.	48
(3) Aerosol Generator.	49
C. Experimental Results.	51
1. Flexible Belt Designs.. . . .	51
2. Rotating and Stationary Cylinder Designs.	58
3. Rotating Disk Designs	63
a. Horizontal Disk	63
b. Inclined Disk	70
D. Particle Size Analysis.	70
V. DISCUSSION OF RESULTS	75
A. General	75

TABLE OF CONTENTS (CONCLUDED)

	Page
B. Effects of Varying Humidity and Particle Contact Area on the Force of Adhesion between a Particle and a Solid Surface	76
C. Feed Velocity Effects and Limiting Particle Sizes by Impaction.	79
D. Verification of Theoretical Results	80
E. Capacity and Recovery Efficiency of Rotating Disk Design	82
VI. CONCLUSIONS.	85
VII. RECOMMENDATIONS	87
VIII. APPENDIX.	89

This report contains 91 pages.

LIST OF FIGURES

	Page
1. Adhesion between a Sphere and a Plane Surface Due to a Liquid Pool.	
2. Factors for Adhesion Theories between Spheres and Plane Surfaces.	9
3. Approximate Adhesion Forces between a Sphere and a Plane Surface	10
4. Adhesion of Two Spherical Surfaces.	12
5. Factors for Adhesion Theories between Two Spherical Surfaces.	14
6. A Particle Suspended from a Horizontal Surface.	17
7. A Particle Adhered to a Vertical Surface.	17
8. Trajectories of Small Particles with Zero Projection Angle	23
9. Trajectories of 36 Micron Diameter Particles with Varying Projection Angles ($V_0 = 50$ m/sec)	24
10. Cross-Section Profiles of the Liquid Pools between a Sphere and a Horizontal Surface and between Two Spheres	28
11. Liquid Pool Profile between a Horizontal Liquid Surface and a Vertical Surface.	31
12. Liquid Pool Profile between a Cylinder and a Horizontal Liquid Surface.	31
13. Cross-Section Profile of Water Surface in Two Dimensional Case by an Analog Computer.	34
14. Flexible Belt Designs.	39
15. Rotating and Stationary Cylinder Designs.	42
16. Rotating Disk Designs	44
17. Photograph of Horizontal Rotating Disk Design	45
18. Air Jet Assembly.	47
19. Vacuum Feed Enclosure	47

LIST OF FIGURES (CONTINUED)

	Page
20. The Wright Dust Feed Mechanism	50
21. Classification of Glass Beads (Fine) by the Flexible Belt Design (Method II)	52
22. Classification of Talc by the Flexible Belt Design (Method II).	54
23. Classification of Glass Beads (Coarse) by the Flexible Belt Design (Method II)	56
24. Classification of Glass Beads (Fine) by the Flexible Belt Design (Method III)	57
25. Classification of Glass Beads (Coarse) by the Flexible Belt Design (Method III)	59
26. Classification of Glass Beads (Fine) by the Flexible Belt Design (Method IV).	60
27. Classification of Glass Beads (Coarse) by the Rotating Cylinder Design.	61
28. Classification of Glass Beads (Fine) by the Rotating Cylinder Design.	62
29. Classification of Glass Beads (Fine) by the Stationary Cylinder Design.	64
30. Classification of CaCO_3 by the Horizontal Rotating Plexiglass Disk.	66
31. Classification of Talc by the Horizontal Rotating Glass Disk	67
32. Classification of ZrO_2 by the Horizontal Rotating Glass Disk	68
33. Classification by Size of a NiO-BaSO_4 Mixture by the Horizontal Rotating Plexiglass Disk.	69
34. Photographs of NiO-BaSO_4 Separation.	71
35. Classification of BaSO_4 by the Plexiglass Inclined Rotating Disk.	72
36. Contact Area between a Conical Particle and a Horizontal Surface	77

LIST OF FIGURES (CONCLUDED)

	Page
37. Dependence of Adhesive Force on Relative Humidity	78
38. Theoretical and Experimental Liquid Profiles.	81
39. Photographs of Water Film Profiles between a Water Surface and a Glass Plate	83

LIST OF TABLES

	Page
I. LIMITING PARTICLE SIZES ADHERED TO A HORIZONTAL SURFACE WITH AN APPLIED VIBRATION.	16
II. LIMITING PARTICLE SIZES ADHERED TO A VERTICAL SURFACE WITH AN APPLIED VIBRATION.	19
III. LIMITING PARTICLE SIZES ADHERED TO A VERTICAL SURFACE WITH AN APPLIED VIBRATION AND CORRECTION FACTOR, $\alpha = 0.1$	20
IV. MAXIMUM PROJECT DISTANCES OF VARIOUS SUB-SIEVE PARTICLES	22
V. SEPARATION OF A NaCl-POWDER PLASTIC BEADS MIXTURE BY THE HORIZONTAL ROTATING DISK.	73

I. SUMMARY

The purpose of this study was to explore a new principle for separating solid particles according to size in the normally subsieve range, and to develop a particle classifier utilizing the adhesive forces acting between particles and a solid surface as a classifying mechanism.

Theoretical studies were made of the magnitude of the adhesive force acting between a spherical particle and a flat surface in the presence of a thin liquid film and of the forces acting between two spherical particles in the presence of a liquid film. Studies were also made of the theoretical cross-sectional profiles of liquid pools between particles and surfaces. Analytical solutions for many of the situations studied were not possible and in most cases it was necessary to resort to an analog computer for the required solutions. Experimental verification of the calculated profiles was obtained for one case.

Theoretical studies were also made of the maximum disturbing force necessary to remove adhered particles from solid surfaces in a number of different orientations. Results were compared for a number of cases and a correction factor, considered to depend on relative humidity, particle shape, surface roughness, electrostatic charge, etc., was proposed to bring theoretical and experimental values into agreement. Theoretical calculations were made of the drag or body forces required to remove adhered particles, and the classifying effect due to the unusual trajectories of small particles. A plausible theory was developed to explain the effects of relative humidity and particle contact area on the forces of adhesion.

Experimental classifiers were constructed according to three primary designs, each consisting basically of a substrate onto which the powder to be classified was placed. The most promising design consisted essentially of a horizontal disk rotating about a vertical axis. The powder, in aerosol form, was impacted onto the underside of the disk through a small jet surrounded by a vacuum feed enclosure. The largest particles rebounded from the disk into collection chambers and the very finest particles followed the fluid streamlines into a collection chamber. Those particles that adhered to the disk were removed by an external air jet and wiping pads. Good classification by size was achieved with all materials tested and classification efficiencies of approximately 90 per cent, based on the coarsest and finest fractions collected, were reported for materials such as CaCO_3 . The mass mean diameter of the finest fraction collected generally ranged from 2 to 5 microns.

Several exploratory experiments indicated that separation of mixtures according to their physical nature might be possible. Further work is needed to explore fully this interesting possibility.

II. INTRODUCTION

In previous studies on the forces of adhesion between particles and surfaces, it has been shown^{1,2,3} that the size distribution of particles adhering to a surface shifts gradually, but regularly, to smaller sizes as the forces tending to dislodge the particles increase. It has also been shown⁴ that a classifying effect may be realized from the unusual trajectories of small particles when their motion is subject to Stokes' law rather than Newton's law. The purpose of this study has been to investigate the use of these techniques as a means of particle size classification in the normally sub-sieve range, i.e., 50 microns to fractional micron diameters.

A number of variables affect the forces of adhesion between solid particles and solid surfaces, among the more important of these are the particle size, shape, area of contact, and the air's relative humidity. Many of the effects of these variables can neither be measured nor controlled and to assess the importance of them on an individual particle basis leads to large uncertainties and variations in actual and predicted behavior. The method of this study has been to evaluate effects on a particle size

-
1. E. Cremer, F. Conrad, and T. H. Kraus, "Die Haftfähigkeit von Pulvern und ihre Anwendung zur Bestimmung von Korngrößen," Angew. Chem. 64, No. 1, p. 10-11 (1952).
 2. M. C. Kordecki, J. K. Gladden, and C. Orr, Jr., Adhesion Between Solid Particles and Solid Surfaces, Final Report, Project No. B-148, Sept. 30, 1959.
 3. B. V. Deryagin and A. D. Zimon, "Adhesion of Powder Particles to Plane Surfaces," Colloid Journal (USSR) 23, No. 5, p. 454-460 (1961).
 4. C. E. Lapple and C. B. Shepherd, "Calculation of Particle Trajectories," Ind. and Eng. Chem. 32, 606-616 (1940).

distribution basis, thus obtaining average values of effects over a large number of particles.. Many interesting aspects of theoretical particle behavior were investigated and important results obtained in new methods of force calculation.

III. THEORETICAL STUDIES OF PARTICLE MECHANICS

A. General Considerations

It is generally recognized that the tenacity with which particles may cling to each other or to other materials is a complex function of such variables as particle size, shape, surface roughness, crystal structure and orientation, dielectric and work constants of the materials involved, relative humidity and adsorbed gases, area of contact, particle deformation, electrostatic charge and London-van der Waals forces.^{5,6,7} It is apparent that some of these variables can neither be measured nor can their effects be controlled. This inability to measure and control certain important variables has previously led to uncertainties and large variations in calculated and experimental values of adhesive forces.

One purpose of this study has been to investigate particle adhesion as a mechanism for particle size classification; therefore, a theoretical study of certain aspects of particle mechanics was undertaken to evaluate the effects of some of the more important variables on particle adhesion and to determine what limiting effects might be expected. Those variables such as particle size, shape, relative humidity, and the presence of disruptive forces, which are obviously important and in some cases may be controlled, are included in the study. Effects such as the presence of electrostatic charge have been minimized by grounding of all

-
5. R. S. Bradley, "The Cohesive Forces Between Solid Surfaces and the Surface Energy of Solids," Phil. Mag. 13, 853-62 (1932).
 6. H. C. Hamaker, "The London-van der Waals Forces Between Spherical Particles," Physica. 4, 1058-72 (1937).
 7. A. P. Prosser and J. A. Kitchener, "Direct Measurement of Long-Range van der Waals Forces," Nature 178, 1339-40 (1956).

equipment and operating at relatively high humidities.

Another area of theoretical and practical importance in surface phenomena is the true curvature of the cross-sectional profile of liquid pools between objects that are joined by these pools. Apparently this subject has received little attention, probably due in part to the generally intractable expressions that describe the profiles. Several cases of interest have been solved with the aid of an analog computer and, in one case, experimental verification of the theoretically predicted profiles has been obtained.

B. Theory of Adhesion between a Sphere and a Plane Surface Due to a Liquid Film.

The pressure inside a liquid surface is generally considered to be less than atmospheric pressure by approximately T/r , where T is the surface tension of the liquid and r is an assumed outside radius of curvature of the liquid surface.^{8,9} Referring to Figure 1, the total force acting over the entire liquid pool according to generally accepted theory is equal to $F_L = \pi a^2 T/r$, and as a first approximation, $a^2 = 4Rr$, although exactly $a = \frac{2\sqrt{rR}}{\frac{r}{R} + 1}$; a derivation of the exact value of a is given in the Appendix. The total adhesive force may therefore be represented approximately as $F_L = 4\pi TR$. Strictly speaking, however, the above theory ignores the following problems:

1. The assumed outside radius of curvature of the liquid surface may not be constant, thus resulting in a noncircular cross section of the liquid pool profile.

8. J. S. McFarlane and D. Tabor, "Adhesion of Solids and the Effect of Surface Films," Proc. Roy. Soc. A202, 224-43 (1950).

9. F. P. Bowden and D. Tabor, The Friction and Lubrication of Solids, Clarendon Press, Oxford, 1950.

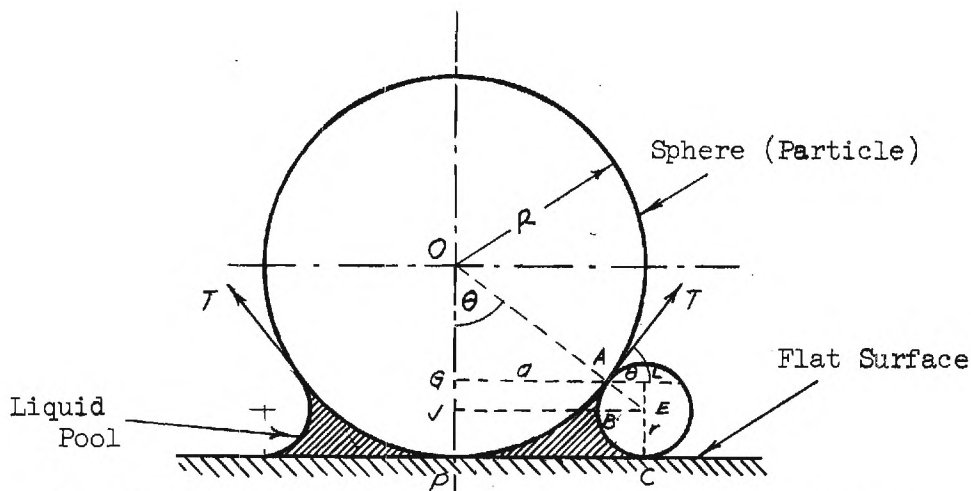


Figure 1. Adhesion between a Sphere and a Plane Surface Due to a Liquid Pool.

2. The true pressure difference between the interior of the liquid pool and the atmosphere is not equal to T/r even if the liquid profile has a constant radius of curvature r . Actually, the liquid surface is a "saddle shape" and the pressure difference should be $T(\frac{1}{r} - \frac{1}{q})$ where q is the radius of curvature of the liquid surface perpendicular to the r plane which is usually larger than the radius r . For example, at point A in Figure 1, $q = R$; at point B, $q = 2\sqrt{Rr - r^2}$; and at point C, $q = \infty$.

3. A direct surface tension force F_2 should be added to the force F_1 established by the pressure difference. This force is expressed by

$$F_2 = 2\pi a T \sin \theta = 2\pi T \frac{a^2}{R} = 8\pi T \frac{r}{(1 + \frac{r}{R})^2} \quad (3.1)$$

When the radius R of a particle is comparable to the radius of curvature r , this force would be comparable in value to the force F_1 .

4. The gravitational force of a liquid pool should also be taken into account in order to calculate accurately the force required to

remove a particle from a surface when the weight of the liquid pool is comparable to the weight of the particle.

C. Calculation of Adhesive Forces Due to Liquid Film between Particles and Surfaces

1. A Sphere and a Plane Surface

In the case of a very thin liquid film, as might be present on a rather dry surface, the radius of curvature of the liquid film is very small and for many purposes can be assumed constant. The approximate force of adhesion may be then written as follows:

$$\begin{aligned} F &= F_1 + F_2 = \pi a^2 \frac{T}{r} + 2\pi a^2 \frac{T}{R} \\ &= \frac{4\pi R T}{\left(1 + \frac{r}{R}\right)^2} + \frac{8\pi r T}{\left(1 + \frac{r}{R}\right)^2} \\ &= 4\pi T R \frac{1 + \frac{2r}{R}}{\left(1 + \frac{r}{R}\right)^2} \\ &= 4\pi T R \left[1 - \frac{\left(\frac{r}{R}\right)^2}{\left(1 + \frac{r}{R}\right)^2} \right] \end{aligned} \quad (3.2)$$

Figures 2 and 3 illustrate some of the properties of equation 3.2. The

factor $4 \left[1 - \frac{\left(\frac{r}{R}\right)^2}{\left(1 + \frac{r}{R}\right)^2} \right]$ is 3 and $F = 3\pi TR$ when $r = R$. Another radius

of curvature q at the contact point between a spherical surface and a

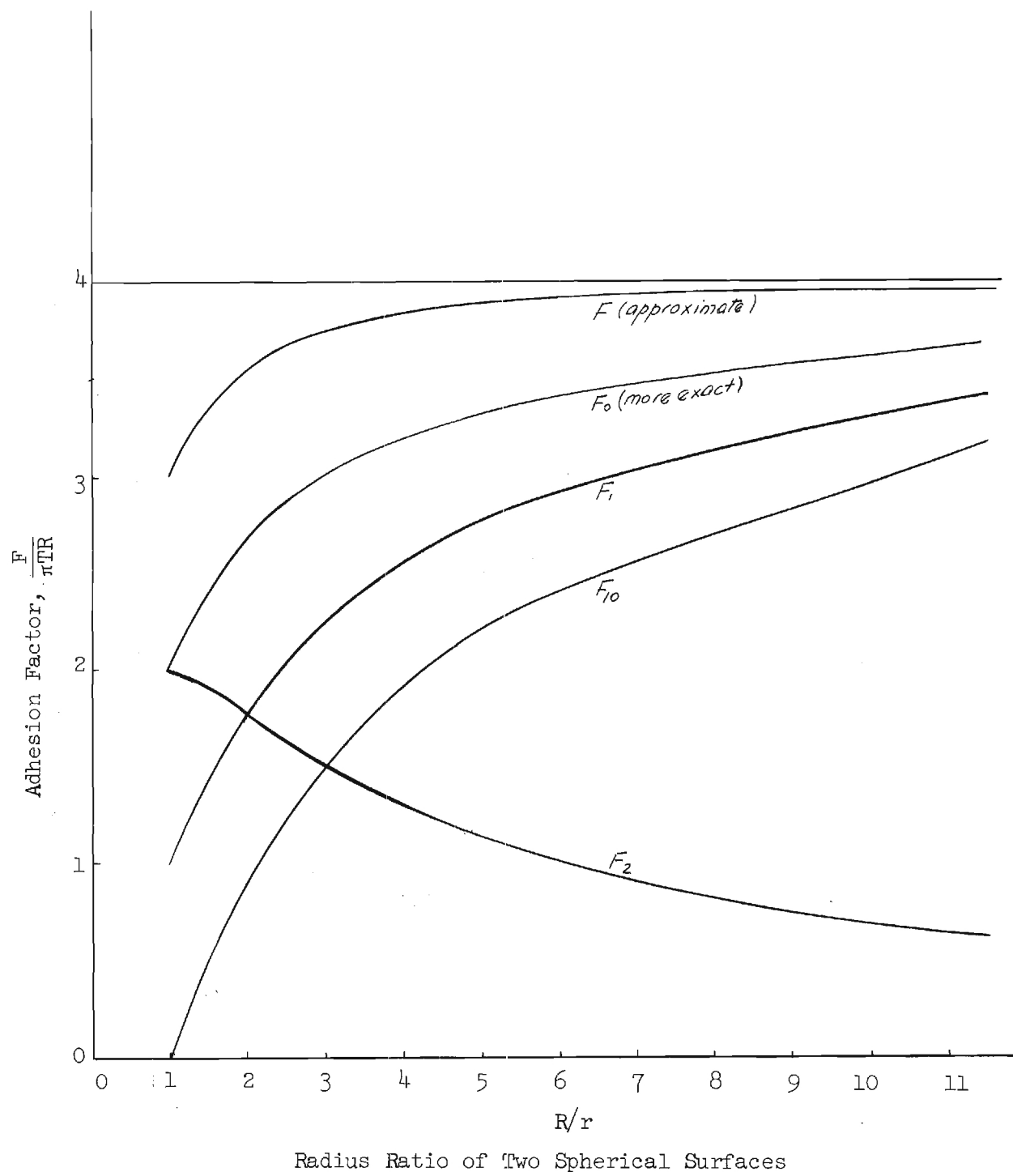


Figure 2. Factors for Adhesion Theories Between Spheres and Plane Surfaces.

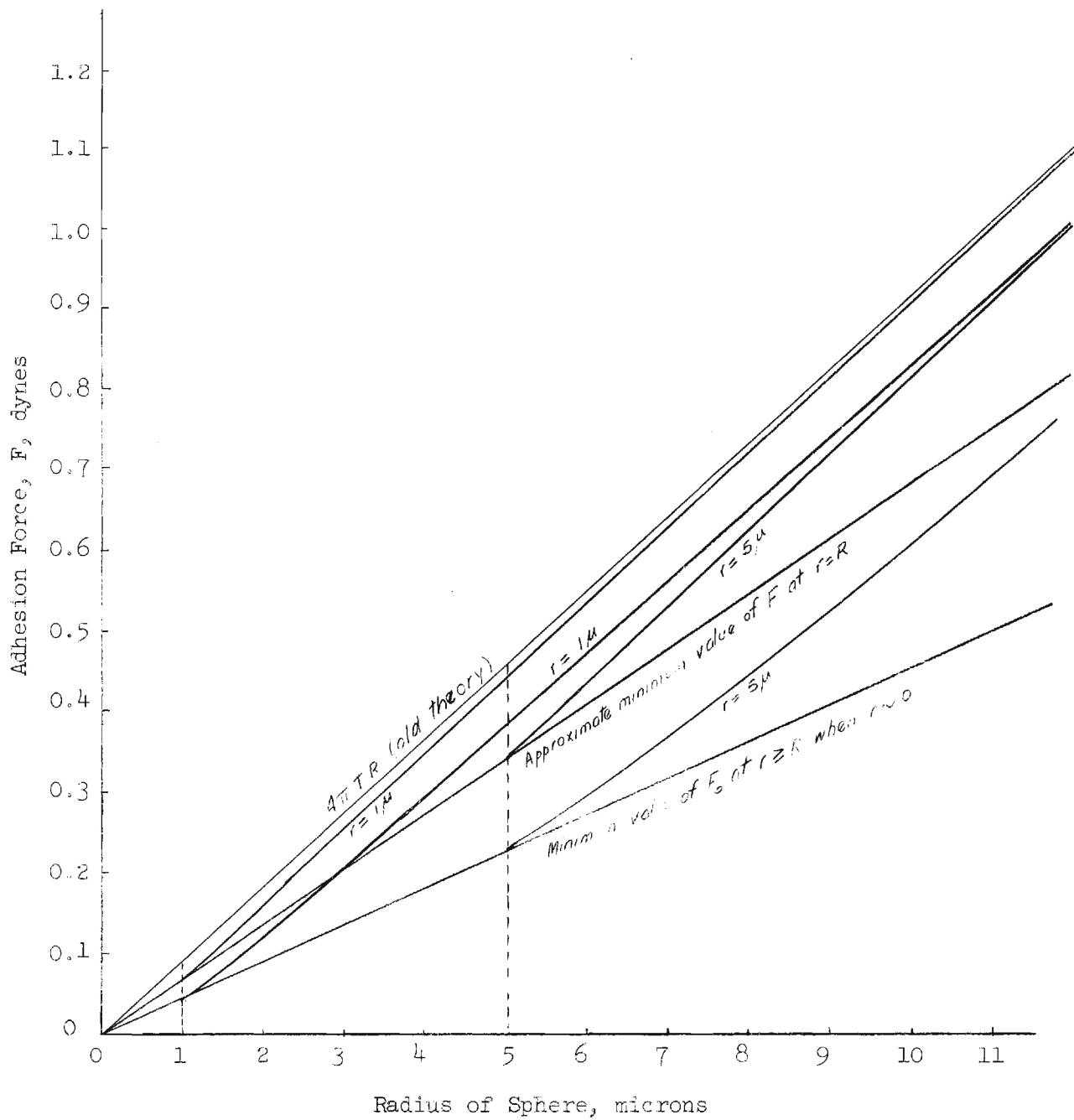


Figure 3. Approximate Adhesion Forces between A Sphere and a Plane Surface.

liquid surface is equal to R and, as a result, the force F_1 should be corrected and called F_{10} as follows:

$$F_{10} = \pi a^2 T \left(\frac{1}{r} - \frac{1}{R} \right) = 4\pi T R \left[\frac{1 - \frac{r}{R}}{\left(1 + \frac{r}{R}\right)^2} \right] \quad (3.3)$$

The resultant force F_0 should be

$$F_0 = F_{10} + F_2 = 4\pi T R \left[\frac{1 + \frac{r}{R}}{\left(1 + \frac{r}{R}\right)^2} \right] \quad (3.4)$$

Equation 3.4 represents a more accurate expression for the force of adhesion than does equation 3.2; although even this expression is not exact as r may not be constant for the entire surface when q is not constant.

For this case the factor of the adhesion force, $4 \left[\frac{1 + \frac{r}{R}}{\left(1 + \frac{r}{R}\right)^2} \right]$

is 2 at $r = R$. These results are also shown in Figures 2 and 3.

The adhesion force F_0 is not directly proportional to the radius of a spherical particle and has a rather steep change when the particle radius approaches that of the liquid film.

2. Between Two Spheres

If a spherical particle adheres to another spherical surface having the same radius of curvature, the force of adhesion F' by a liquid film can be approximately calculated by the following equations. Figure 4 illustrates this situation.

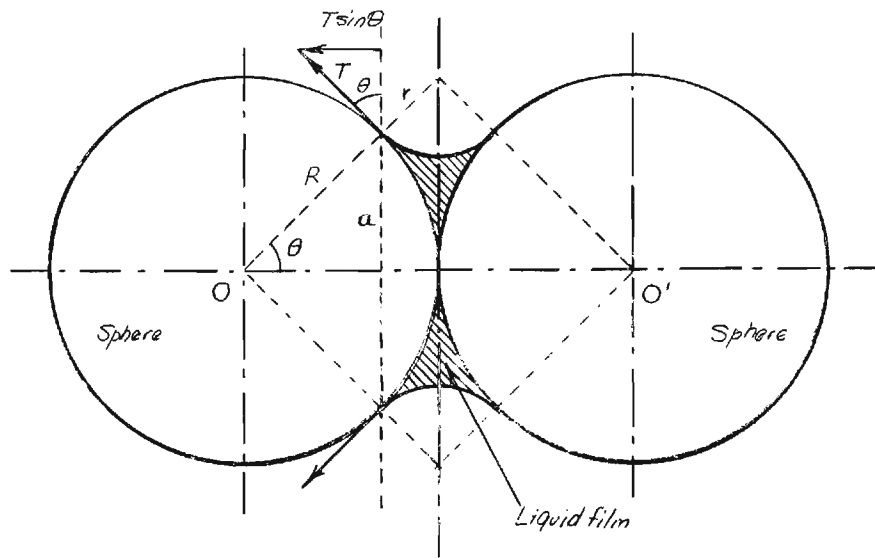


Figure 4. Adhesion of Two Spherical Surfaces.

$$a = R \sqrt{1 - \frac{1}{\left(1 + \frac{r}{R}\right)^2}} \quad (3.5)$$

$$F_1' = \pi a^2 \frac{T}{r} = \pi T \frac{R^2}{r} \left[1 - \left(\frac{1}{1 + \frac{r}{R}} \right)^2 \right] \quad (3.6)$$

(force by pressure difference)

$$F_2' = 2\pi a T \sin \theta = 2\pi R T \left[1 - \left(\frac{1}{1 + \frac{r}{R}} \right)^2 \right] \quad (3.7)$$

(force by surface tension)

$$\therefore F' = F'_1 + F'_2 = \pi T R \left(\frac{R}{r} + 2 \right) \left[1 - \left(\frac{1}{1 + \frac{r}{R}} \right)^2 \right] \quad (3.8)$$

The following tabulation gives expressions for the individual and cumulative forces for typical values of the radius ratio of the sphere and water film.

R/r	F'_1	F'_2	F'
0	0	$2 \pi T R$	$2 \pi T R$
1	$3/4 \pi T R$	$3/2 \pi T R$	$9/4 \pi T R$
∞	$2 \pi T R$	0	$2 \pi T R$

Equation 3.8 is plotted in Figure 5, and has a maximum at $r = R$. Strictly speaking, especially in the case of a small particle ($r \approx R$), this is not correct and should be corrected to the more accurate expression F'_{10} .

$$F'_{10} = \pi a^2 T \left(\frac{1}{r} - \frac{1}{R} \right) = \pi T R \left(\frac{R}{r} - 1 \right) \left[1 - \frac{1}{\left(1 + \frac{r}{R} \right)^2} \right] \quad (3.9)$$

It follows therefore that

$$F'_0 = F'_{10} + F'_2 = \pi T R \left(\frac{R}{r} + 1 \right) \left[1 - \frac{1}{\left(1 + \frac{r}{R} \right)^2} \right] \quad (3.10)$$

Results calculated by equation 3.10 are also shown in Figure 5. The adhesion force F'_0 is not directly proportional to the particle radius R when $R \approx r$ and is always smaller than the adhesion force F_0 between a sphere and a flat surface.

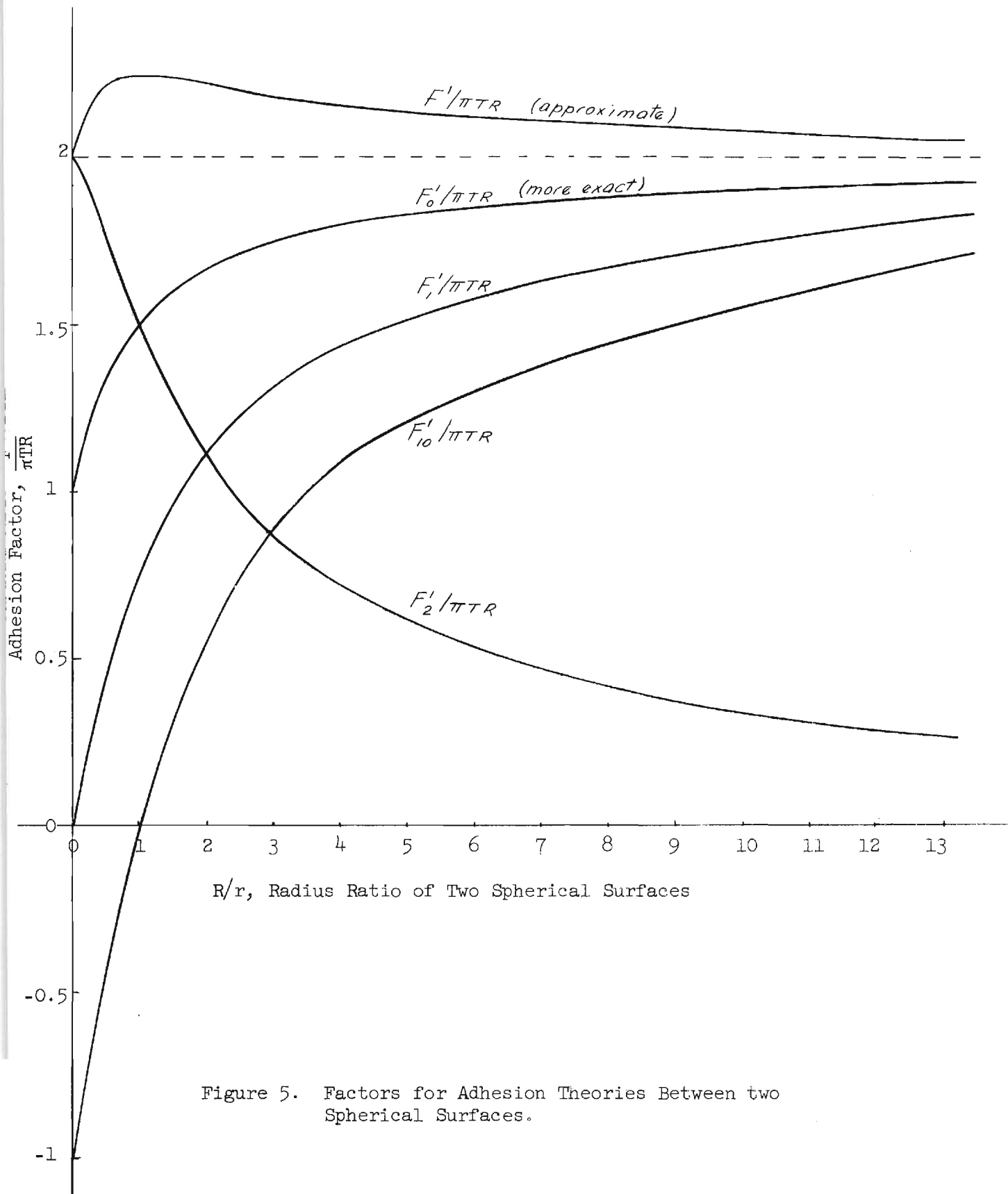


Figure 5. Factors for Adhesion Theories Between two Spherical Surfaces.

This theory, while an improvement over earlier ones, is not exact since the radius of curvature r is not constant, especially in the case of two spheres, even when the radius of curvature r is very small ($r \approx R$). In this case as in the previous one, the radius of curvature q is not constant and \underline{a} cannot be obtained exactly from the given equations.

D. Calculation of Limiting Particle Sizes for Adhesion to Horizontal and Vertical Plane Surfaces

1. Horizontal Surfaces

The following equation is obtained from a vertical force balance on the system illustrated in Figure 6.

$$W = F_1 + F_2$$

or

$$\frac{4}{3} \pi R^3 \rho_s g = 4\pi T R \left[\frac{1 + \frac{r}{R}}{(1 + \frac{r}{R})^2} \right] \quad (3.11)$$

where g = gravitational constant and ρ_s = density of the particle.

Usually $r \ll R$, then F_2 is negligibly small, and

$$R \approx \sqrt{\frac{3T}{\rho_s g}} \quad (3.12)$$

When the liquid is water, $T = 73$ dyne/cm, and if $\rho_s = 2.5$ g/cm³.

$$R = \sqrt{\frac{3 \times 73}{2.5 \times 980}} \approx 0.30 \text{ cm} = 3.0 \text{ cm}$$

This size corresponds to the largest particle which will not fall from a horizontal surface. If a sinusoidal vibration is applied to this system, the following equation is obtained at the critical condition.

$$\left(\frac{4}{3} \pi R^3 \rho_s\right) 4\pi^2 h p^2 + \left(\frac{4}{3} \pi R^3 \rho_s\right) g = 4\pi T R \frac{1 + \frac{r}{R}}{\left(1 + \frac{r}{R}\right)^2} \quad (3.13)$$

(maximum vibration force) (gravity force) (adhesion force)

When $r \ll R$, then

$$R \approx \sqrt{\frac{3T}{\rho_s (g + 4\pi^2 h p^2)}} \text{ cm} \quad (3.14)$$

where h = one-half of the vibration amplitude in cm, and p = vibration frequency in cycles/sec. When $T = 73/\text{dyne cm}$, $\rho_s = 2.5 \text{ g/cm}^3$, and $p = 60 \text{ cycles/sec}$, Table I is obtained from equation 3.14.

TABLE I
LIMITING PARTICLE SIZES ADHERED TO A HORIZONTAL SURFACE
WITH AN APPLIED VIBRATION

h , cm	0.01	0.10	1.00	2.78	27.8	278
hp^2 , cm/sec ²	36	360	3600	10^4	10^5	10^6
R , microns	1910	759	247	149	47	15

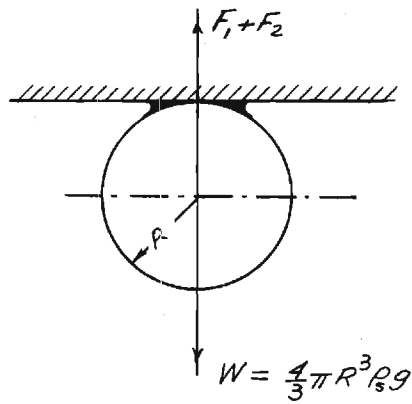


Figure 6. A Particle Suspended from a Horizontal Surface.

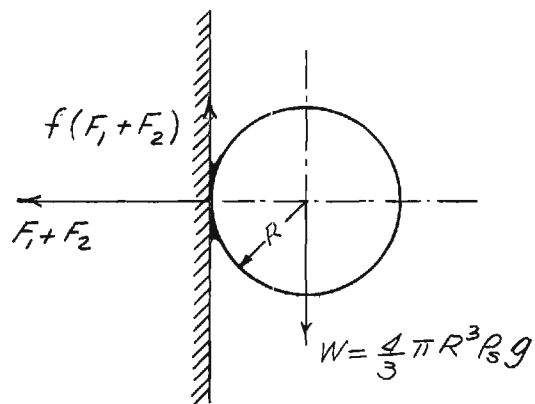


Figure 7. A Particle Adhered to a Vertical Surface.

2. Vertical Surfaces

The frictional force acting between a particle and a surface is balanced by the gravity force on the particle. A force balance on the system illustrated in Figure 7 on the preceding page then yields the following equation

$$W = f (F_1 + F_2)$$

or

$$\left(\frac{4}{3} \pi R^3 \rho_s\right) g = 4\pi f T R \left[\frac{1 + \frac{r}{R}}{\left(1 + \frac{r}{R}\right)^2} \right] \quad (3.15)$$

where f is a friction factor.

Usually $r \ll R$, and

$$R \approx \sqrt{\frac{3fT}{\rho_s g}} \quad (3.16)$$

When $T = 73$ dyne/cm, $\rho_s = 2.5$ g/cm³, and $f = 0.7$

$$R = \sqrt{\frac{3 \times 73 \times 0.7}{2.5 \times 980}} \approx 0.095 \text{ cm} \approx 0.95 \text{ mm}$$

or

$$D_p = 2R \approx 1.9 \text{ mm}$$

This size corresponds to the largest particle which can adhere to a vertical surface, and is \sqrt{f} times the largest particle size suspended from a horizontal surface. If the same vibration as in the preceding case is applied, the following result is obtained.

$$R \approx \sqrt{\frac{3fT_v}{\rho_s (g + 4\pi^2 h p^2)}} \text{ cm} \quad (3.17)$$

When the same conditions as previously used apply and it is assumed that $f = 0.1$, Table II values are obtained from equation 3.17.

TABLE II
LIMITING PARTICLE SIZES ADHERED TO A VERTICAL SURFACE
WITH AN APPLIED VIBRATION

hp^2 , cm	10	50	100	500	3600	5000	10^5	10^6
R, microns	796	543	423	204	78	66	15	5

The calculated results of cut sizes, R, are larger than experimental values.¹⁰ If a reduced adhesion force is calculated by use of a correction factor α , which is considered to depend on particle shape, size, roughness, relative humidity, etc., a reasonable result may be obtained as follows.

$$R = \sqrt{\frac{3f \alpha t}{\rho_s (g + 4\pi^2 h p^2)}} \quad (3.18)$$

where $f = 1$ at a horizontal surface, and f is assumed to be between 0 and 1 at a vertical surface. If α is assumed to be 0.1, the values given in Table III are obtained using the same conditions as previously stated. These values are in reasonable agreement with experimental values.

10. R. I. Larsen, "The Adhesion and Removal of Particles Attached to Air Filter Surfaces," presented at the Air Pollution-Engineering Section of the Am. Industrial Hygiene Assn. Annual Meeting in Atlantic City, New Jersey, April 24, 1958.

TABLE III

LIMITING PARTICLE SIZES ADHERED TO A VERTICAL SURFACE
WITH AN APPLIED VIBRATION AND CORRECTION FACTOR, $\alpha = 0.1$

h, cm	0.01	0.10	1.00	2.78	27.8	278
R, microns	191	76	25	15	5	1.5

E. Calculation of the Classifying Effect Arising from the Trajectories of Bounced Particles

Very small particles, when bounced from surfaces or projected from a jet, have trajectories that are strongly size dependent and that show unusually sharp turns since their motion is governed by Stokes' law rather than Newton's law. The following equations of motion for a small particle are readily derived by elementary force balances:

$$m \ddot{x} + 3\pi \mu \delta \dot{x} = 0 \quad (3.19)$$

$$m \ddot{y} + 3\pi \mu \delta \dot{y} = mg \quad (3.20)$$

where m is the mass of the particle, x is the abscissa of particle motion, y is the ordinate of particle motion, μ is the fluid viscosity, δ is the particle diameter, g is the gravitational constant, and \dot{x} and \dot{y} denote the first derivatives of x and y with respect to time.

The initial conditions of particle motion at $t = 0$, $x = 0$, and $y = 0$ are $\dot{x} = v_0 \cos \beta$ and $\dot{y} = v_0 \sin \beta$, where v_0 is the projection velocity at angle β with the horizontal. If we let $a = \frac{3\pi\mu\delta}{m} = \frac{18\mu}{\rho\delta^2}$

where ρ is the particle density then the solutions to the equations of motion are

$$x = \frac{v_o \cos \beta}{a} (1 - e^{-at}) \quad (3.21)$$

$$y = (v_o \sin \beta + \frac{g}{a}) \frac{1}{a} (1 - e^{-at}) - \frac{g}{a} t \quad (3.22)$$

or

$$y = (v_o \sin \beta + \frac{g}{a}) \frac{x}{v_o \cos \beta} + \frac{g}{a^2} \ln (1 - \frac{ax}{v_o \cos \beta}) \quad (3.23)$$

$$t = \frac{1}{a} \ln \frac{v_o \cos \beta}{v_o \cos \beta - ax} \quad (3.24)$$

The maximum length of projection is $v_o \cos \beta$ and this value does not change appreciably for a given particle diameter even if the projection angle varies considerably. The horizontal component of the particle velocity is seen to depend linearly on projection distance from the following equations:

$$\dot{x} = v_o \cos \beta e^{-at} = v_o \cos \beta - ax \quad (3.25)$$

$$\dot{y} = (v_o \sin \beta + \frac{g}{a}) e^{-at} - \frac{g}{a} = v_o \sin \beta e^{-at} - \frac{g}{a} (1 - e^{-at}) \quad (3.26)$$

Table IV presents the very strong dependence of projection distance on particle size.

TABLE IV

MAXIMUM PROJECTED DISTANCES OF VARIOUS SUB-SIEVE PARTICLES

						Remarks
δ , microns	36	18	9	3	1	$\rho = 2.5 \text{ gm/cm}^3$
a , sec^{-1}	100	401	1605	14,444	130,000	$\mu = 0.0018 \text{ gm/cm-sec}$
x_{max} , cm	300	75	19	2.1	0.23	$v_o = 300 \text{ m/sec}, \beta = 0$

Some calculated trajectories are also shown in Figures 8 and 9. It is apparent that the trajectories are extraordinarily affected by particle size; however, it should be kept in mind that the larger particle sizes are in the transition region from Stoke's behavior to Newton's behavior and the strong size dependence of trajectories may begin to break down in this range.

F. Calculation of the Drag Force Required to Remove Small Adhered Particles from Surfaces

The fluid velocity required to remove adhered particles from a surface may be estimated from a consideration of the fluid mechanics involved. The force exerted on a particle in a flowing stream may be calculated from

$$F = f_d A \rho v^2 / 2 \quad (3.27)$$

where F is the force on the particle, A is the cross-sectional area of the particle, ρ is the fluid density, v is the velocity of the fluid, and f_d is a drag coefficient, which for laminar flow is given by

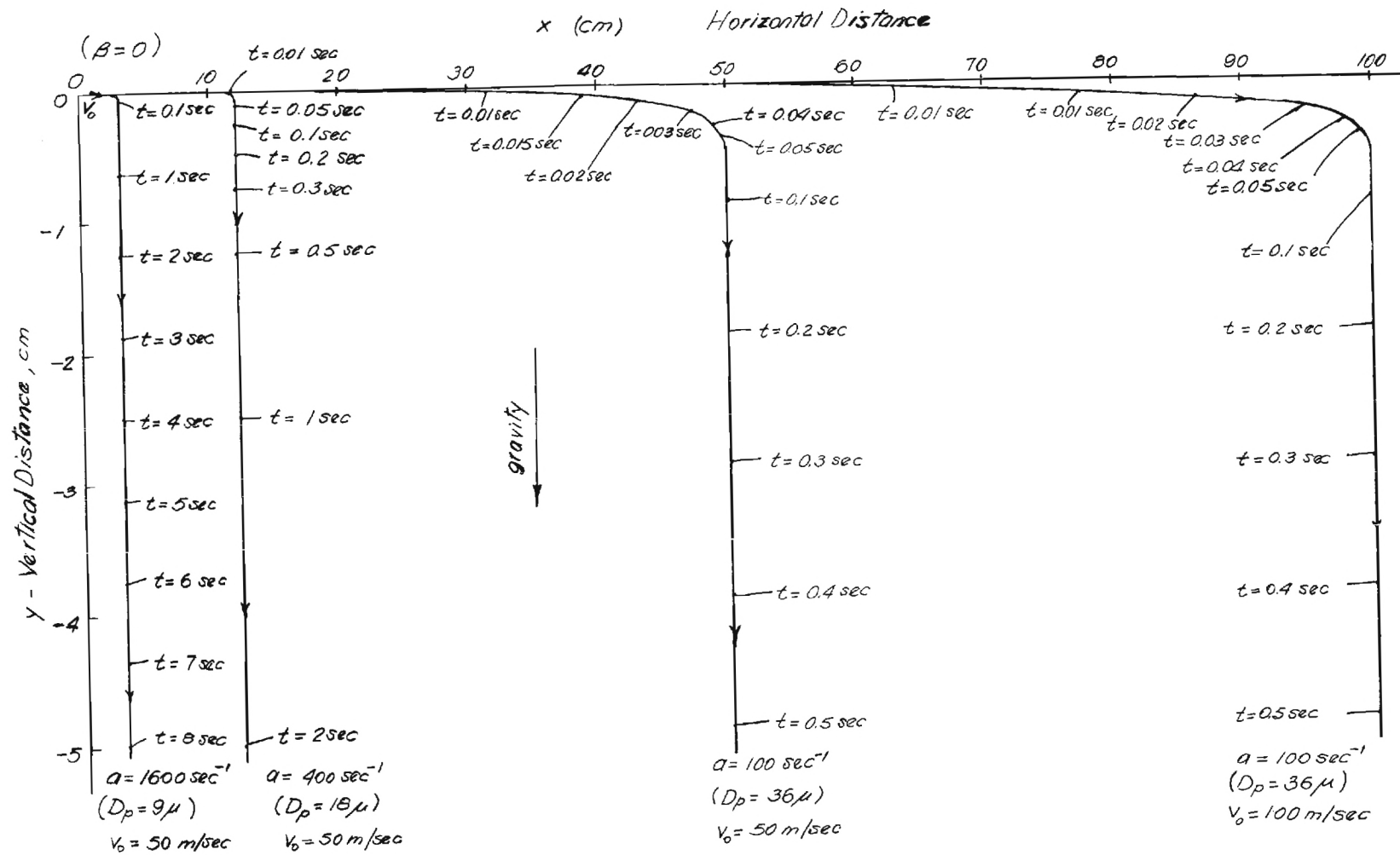


Figure 8. Trajectories of Small Particles with Zero Projection Angle.

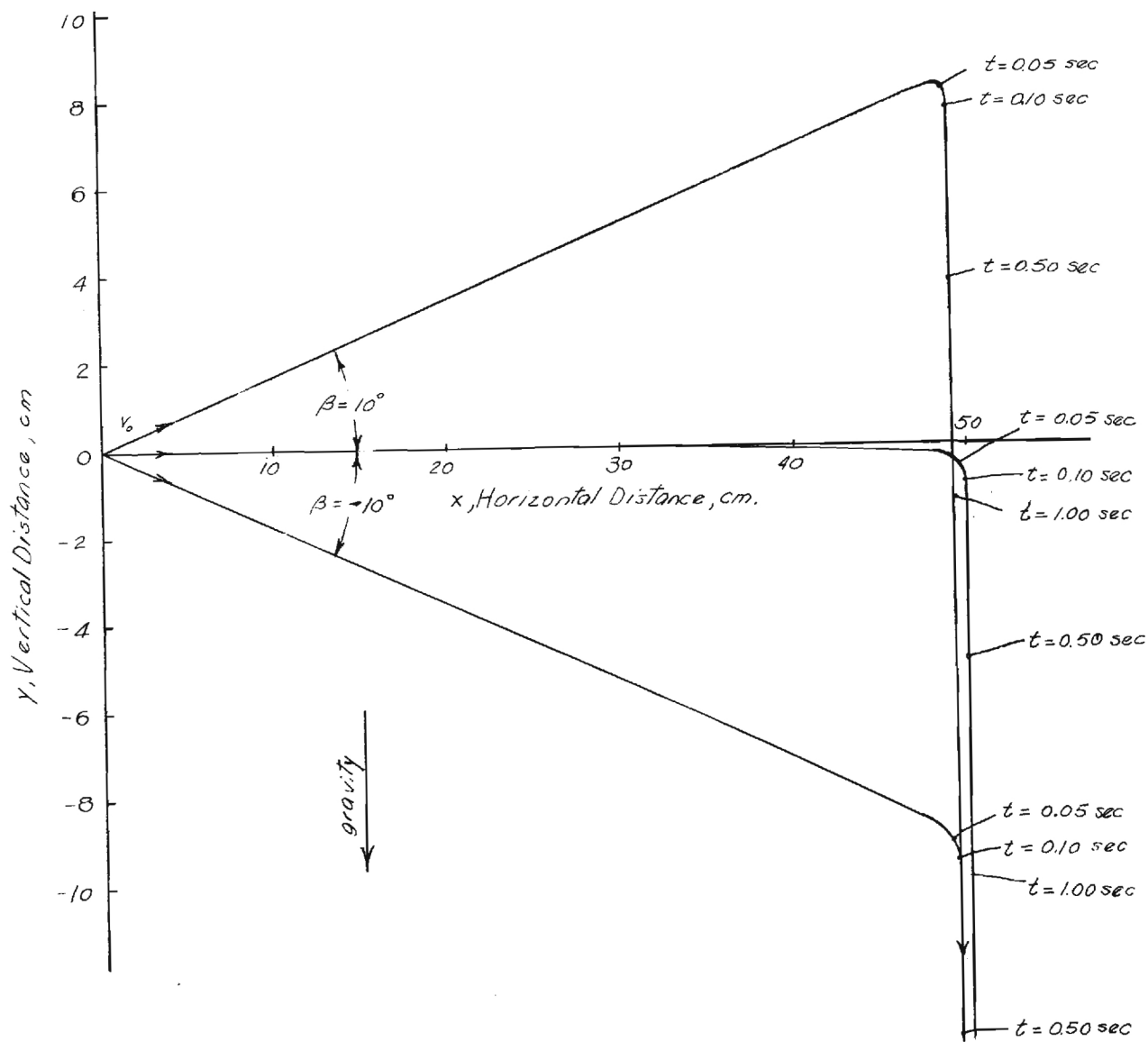


Figure 9. Trajectories of 36 Micron Diameter Particles with Varying Projection Angles ($V_0 = 50 \text{ m/sec}$).

$$f_d = \frac{24 \nu}{\delta} \quad (3.28)$$

if δ is the particle diameter and ν is the kinematic fluid viscosity. A valid expression for the fluid velocity profile near the surface on which the particle rests is given by Bird, Stewart and Lightfoot¹¹ as

$$\frac{v}{v_\infty} = \frac{3}{2} \left(\frac{y}{\epsilon}\right) - \frac{1}{2} \left(\frac{y}{\epsilon}\right)^3 ; \quad 0 \leq y \leq \epsilon \quad (3.29)$$

where v is the fluid velocity at a point y near the surface in the boundary layer of the fluid, v_∞ is the free stream velocity, and ϵ is the boundary layer thickness along the plate. An expression for the boundary layer thickness is also given by Bird, Stewart, and Lightfoot¹² as

$$\epsilon = \frac{4.64 x^{1/2} \nu^{1/2}}{v_\infty^{1/2}} \quad (3.30)$$

where x is the distance along the surface from the leading edge. Substituting equation 3.28 into equation 3.27 and differentiating gives

$$dF = (3\pi \rho \delta \nu) dv \quad (3.31)$$

Differentiating equation 3.29 gives

$$dv = \frac{3v_\infty}{2\epsilon} \left[1 - \left(\frac{y}{\epsilon}\right)^2 \right] dy \quad (3.32)$$

11. R. B. Bird, W. E. Stewart, E. N. Lightfoot, Transport Phenomena, p. 145, Wiley, New York, 1960.

12. Ibid.

Substituting equation 3.32 into 3.31 and integrating over the boundary layer thickness yields an expression for the force in terms of the particle diameter and boundary layer thickness.

$$\int_0^F dF = \frac{K\delta}{\epsilon} \int_0^{\delta} \left[1 - \left(\frac{y}{\epsilon}\right)^2 \right] dy \quad (3.33)$$

where $K = \frac{9\pi \nu \rho v_{\infty}}{2}$

$$F = \frac{K\delta}{3\epsilon} \left[3 - \left(\frac{\delta}{\epsilon}\right) \right] \quad (3.34)$$

but $\epsilon = 4.64 \frac{x^{1/2} \nu^{1/2}}{v_{\infty}^{1/2}}$, and substituting in equation 3.34 yields

$$F = \left[\frac{9\pi \rho \delta^2 \nu^{1/2}}{9.28 x^{1/2}} - \frac{3\pi \rho \delta^4 v_{\infty}}{(4.64)^2 (9.28) x^{3/2} \nu^{1/2}} \right] v_{\infty}^{3/2} \quad (3.35)$$

This rather cumbersome expression may not be solved explicitly for v_{∞} but it can be solved by a trial and error process for known values of the adhesion force F . It is obvious from inspection of equation 3.35 that the fluid velocity required to dislodge very small particles that can immerse in the boundary layer depends on the square and fourth power of the particle size; however, it is difficult to generalize on these effects when other uncertainties such as x , the length of boundary layer buildup, cannot be known in most cases with any degree of certainty, particularly if the air jet is directed onto an irregular surface at some angle.

The actual velocity and corresponding drag force required to dislodge particles will be somewhat less than the theoretical value since the drag force and the adhesion force are acting at right angles. An additional friction factor should be included in the expression for the velocity to bring theoretical and experimental values into agreement. Corn and Silverman¹³ have calculated the drag force required to remove particles from a solid surface by a turbulent air stream. Air drag on particles was calculated assuming a simple irrotational flow model in which the particles were completely immersed in the laminar boundary layer. Air drag forces calculated in this manner were an order of magnitude lower than particle-to-surface adhesion forces determined in a companion study.

G. Calculation of the Theoretical Cross-Section Profiles of Liquid Pools between Particles and Surfaces

1. A Sphere and a Plane Surface, or Two Spheres

The profiles shown in Figure 10 may be described by the following equations which are derived by a force balance over the liquid pool:

$$\left(\frac{1}{r} - \frac{1}{q}\right) T = \Delta p = p_o + \rho g y \quad (3.36)$$

$$r = \frac{\pm (1 + y^2)^{3/2}}{y} > 0 \quad (3.37)$$

13. Morton Corn and Leslie Silverman, "Removal of Solid Particles from a Solid Surface by a Turbulent Air Stream," American Industrial Hygiene Journal, 337 (October 1961).

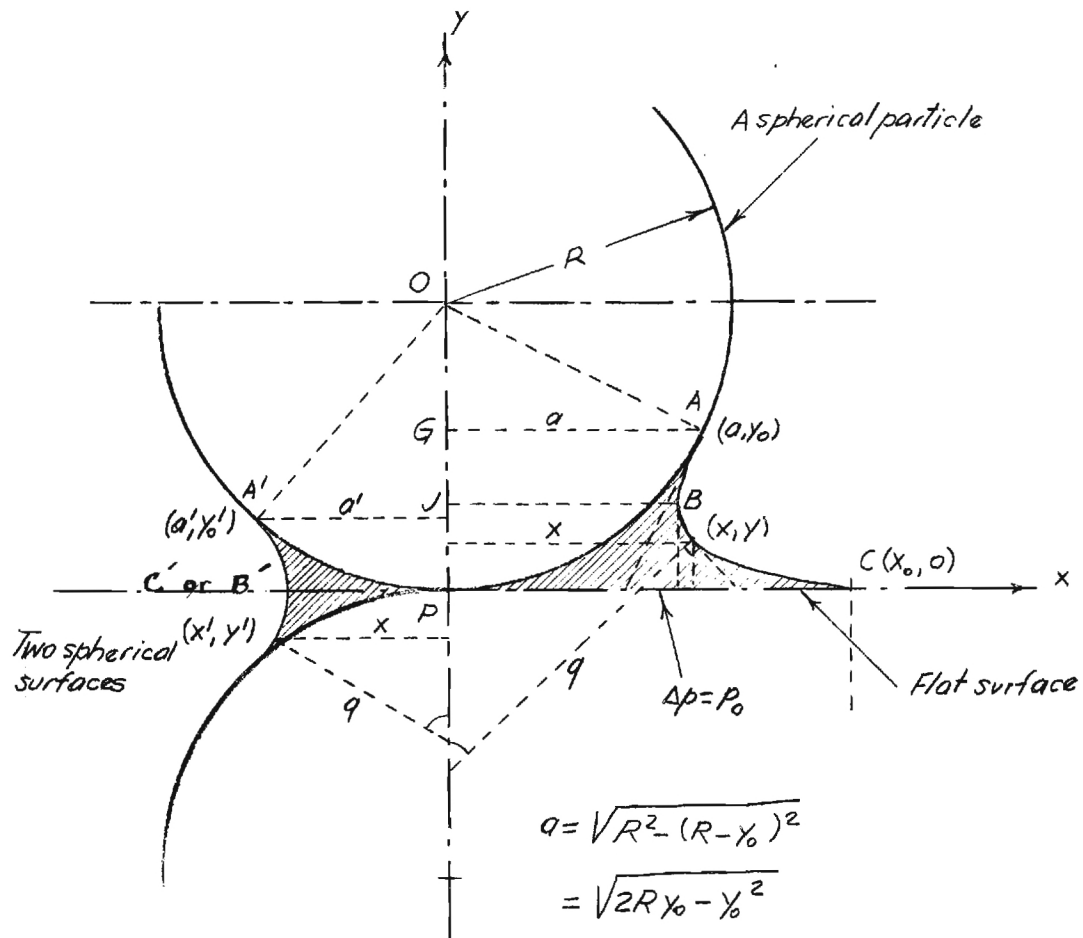


Figure 10. Cross-Section Profiles of the Liquid Pools between a Sphere and a Horizontal Surface and between Two Spheres.

$$q = \frac{x}{\sin(\pi - \phi)} = \frac{x}{\sin \phi} > 0 \quad (3.38)$$

$$\tan \phi = \dot{y} \quad (3.39)$$

Where \dot{y} denotes the derivative of y with respect to x and p_o is the pressure inside the liquid pool at $y = 0$. The boundary conditions for several cases are

a. A particle and a flat surface (right side of Figure 10)

$$\text{at Point A, } q = R, \dot{y} = \frac{a}{R - y_o}; \quad x = a, \quad y = y_o$$

$$\text{at Point B, } q = \overline{BJ}, \dot{y} = \infty$$

$$\text{at Point C, } q = \infty, \dot{y} = 0; \quad x = x_o, \quad y = 0$$

b. Two particles of the same size, (left side of Figure 10)

$$\text{at point A', } q = R, \dot{y} = \frac{a'}{R - y_o}; \quad x = a', \quad y = y_o'$$

$$\text{at point B' or C', } q = \overline{B'P}, \dot{y} = \infty, \quad y = 0$$

from equations 3.38 and 3.39

$$q = x \sqrt{1 + \cot^2 \phi} = x \sqrt{1 + \frac{1}{\dot{y}^2}} = \pm \frac{x}{\dot{y}} \sqrt{1 + \dot{y}^2} > 0 \quad (3.40)$$

and from equations 3.36, 3.37, and 3.40

$$\frac{\pm \ddot{y}}{(1 + \dot{y}^2)^{3/2}} \pm \frac{\dot{y}}{x \sqrt{1 + \dot{y}^2}} = \frac{\Delta p}{T} = \frac{p_o + \rho g y}{T} \quad (3.41)$$

This equation cannot be solved analytically, but may be solved numerically.

If $y \gg 1$, then the following approximate equation results

$$y = -y^3 \left[\frac{1}{x} + \frac{p_o + \rho g y}{T} \right] \quad (3.42)$$

However, if $y \approx 0$, then

$$y + \frac{y}{x} + \frac{p_o + \rho g y}{T} = 0 \quad (3.43)$$

2. A Vertical Plane, or a Cylinder, and a Horizontal Liquid Surface

If the radius of curvature r of the profile surface shown in Figure 11 or Figure 12 is assumed constant, then equilibrium between the gravity force and the surface tension yields the following equation, assuming a unit width of the liquid pool and zero contact angle.

$$\rho g r^2 \left(1 - \frac{\pi}{4}\right) = T$$

or

$$r = \sqrt{\frac{T}{0.215 \rho g}} \quad (3.44)$$

When the liquid is water at normal conditions, the surface tension is about 73 dynes/cm and

$$r = \sqrt{\frac{73}{(0.215)(1)(980)}} = \sqrt{0.347} = 0.59 \text{ cm}$$

Strictly speaking, however, the radius r is not constant, but is determined by the equilibrium of pressures between both sides of the liquid surface.

The corrected liquid profile may be described by the following equations:

$$\frac{T}{r} = \rho g y \quad (3.45)$$

$$r = \frac{\pm (1 + y^2)^{3/2}}{y} \quad (3.46)$$

and the boundary conditions are $y = 0$; $\dot{y} = 0$, and $x = 0$, $\dot{y} = \infty$.

Substituting equation 3.46 into equation 3.45 gives:

$$\frac{T}{\rho g y} = \pm \frac{(1 + y^2)^{3/2}}{y} \quad (3.47)$$

or

$$\pm \frac{T}{\rho g} \frac{\dot{y} \ddot{y}}{(1 + y^2)^{3/2}} = y \ddot{y}$$

Integrating the above equation gives

$$\pm \frac{T}{\rho g} \frac{1}{\sqrt{1 + y^2}} = \frac{y^2}{2} + C_1,$$

and with the boundary condition: $y = 0$; $\dot{y} = 0$,

$$C_1 = - \frac{T}{\rho g},$$

then

$$\pm \frac{1}{\sqrt{1 + y^2}} = 1 - \frac{\rho g y^2}{2T} \quad (3.48)$$

or

$$y^2 = \frac{2T}{\rho g} \left[1 \pm \frac{1}{\sqrt{1 + y^2}} \right]$$

This equation cannot be solved analytically but may be solved numerically or by an analog computer. The initial condition or point of contact is obtained as follows:

$$\text{at } x = 0; \dot{y} = -\cot \beta$$

where β is the contact angle between the solid surface and the liquid, and when the liquid is water, $\beta = 0$, i.e., $\dot{y} = \infty$; then from equation 3.48

$$y_{x=0} = \sqrt{\frac{2T}{\rho g}} = \sqrt{\frac{2 \times 73}{1 \times 980}} = 3.86 \text{ mm} \quad (3.49)$$

The result from an analog computer is given in Figure 13. The upper part of the profile, i.e., above the vertical slope, corresponds to the case of a large cylinder. In the latter case, the maximum value of y for water is obtained from equation 3.48

$$y_{\max} = \sqrt{\frac{4T}{\rho g}} = \sqrt{\frac{4 \times 73}{1 \times 980}} = 5.46 \text{ mm} \quad (3.50)$$

This corresponds to the maximum distance between a horizontal plane and a water surface in which water may be held by surface tension.

The equation of the cylinder depicted in Figure 12 is

$$x'^2 + (R - y')^2 = R^2$$

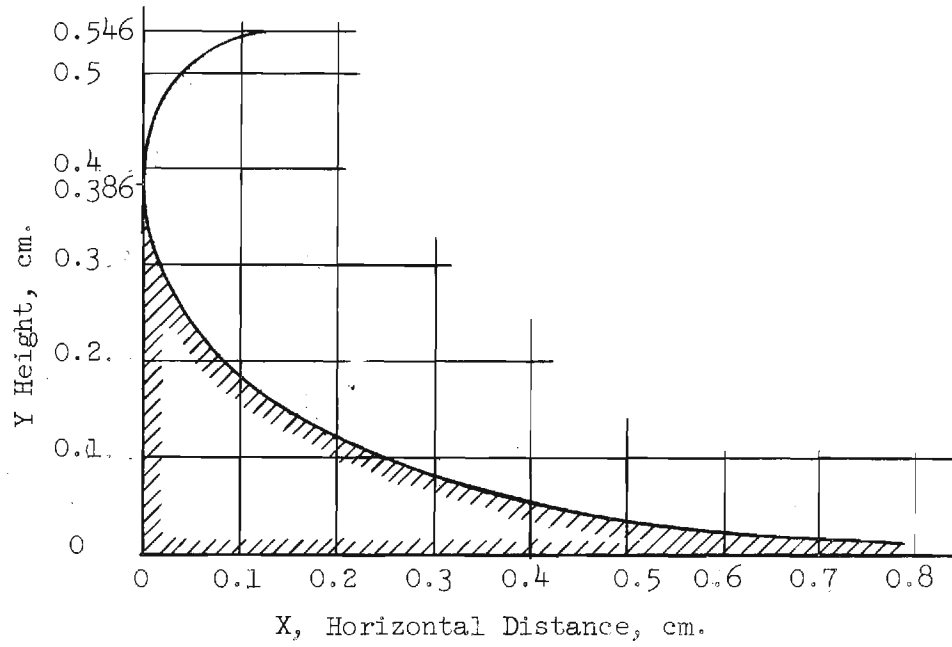


Figure 13. Cross-Section Profile of Water Surface in Two Dimensional Case by an Analog Computer.

and at the contact point, $A(a, y_0)$,

$$\tan \theta = \frac{dy'}{dx'} = \frac{a}{R - y_0}$$

Substituting this value into equation 3.48 and using the negative sign,

$$\sqrt{\frac{-1 + \frac{a^2}{(R - y_0)^2}}{1 + \frac{a^2}{(R - y_0)^2}}} = 1 - \frac{\rho g}{2T} y_0^2$$

$$\therefore \frac{\rho g R}{2T} y_0^2 + y_0 - 2R = 0 \quad (3.51)$$

or

$$y_0 = \frac{-1 + \sqrt{1 + \frac{4\rho g R^2}{T}}}{\frac{\rho g R}{T}}$$

The following coordinates are obtained from equation 3.51 for various cylinder diameters and with water as the liquid

$R, \text{ cm}$	0.386	0.5	1.0	2.0	∞
$y_0, \text{ cm}$	0.386	0.417	0.477	0.509	0.546
$x_0, \text{ cm}$	0.386	0.493	0.852	1.333	--

The same results as given by equation 3.51 may also be derived from the equilibrium of horizontal force components acting on the water profile as follows:

horizontal outward component by surface tension =

$$T \sin \theta + T = \left[1 + \frac{R - y_o}{R} \right] T \quad (3.52)$$

horizontal inward component by pressure difference =

$$\int_0^{y_o} \rho g y \, dy = \frac{\rho g}{2} y_o^2 \quad (3.53)$$

Equating the two values above gives the same expression as equation

3.51.

$$\frac{\rho g R}{2T} y_o^2 + y_o - 2R = 0 \quad (3.54)$$

IV. EXPERIMENTAL TECHNIQUES AND RESULTS

A. General Procedure

The powder to be classified was applied to any one of several types of surfaces by specially constructed feeding devices. All equipment was grounded to minimize the effects of electrostatic charge. Once the powder was on the surface it was subjected to various types of disruptive forces according to the mechanical design employed.

At least two and usually from three to six cuts or size fractions were obtained from each system. The collected material was then analyzed for particle size distribution by optical microscope, optical micrographs, the Sharples micromerograph, or the Coulter counter depending on the size range involved and the amount of collected material available. These distributions were then plotted and compared with the size distributions of the starting materials.

B. Types of Apparatus

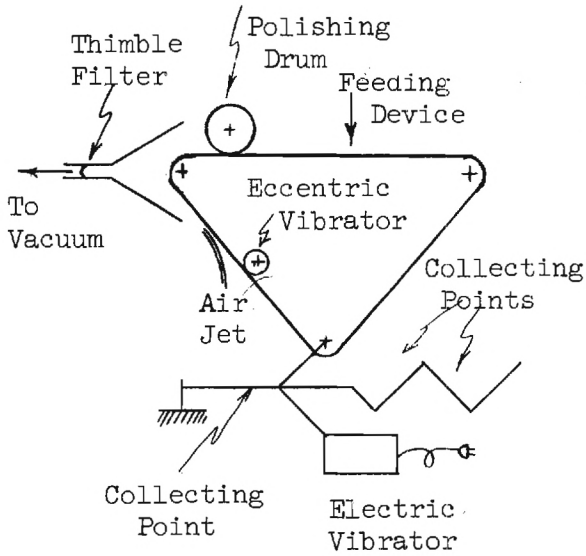
1. Flexible Belt Design

a. Method I. The first type of experimental apparatus used in this study consisted of a flat belt moving around three pulleys mounted with their axes horizontal and arranged in a triangular pattern. The powder to be classified was applied to a horizontal portion of the moving belt by various types of feeding devices. As the belt passed over the driving pulley and began its descent, the coarser particles that were not adhered or only lightly adhered to the belt fell off into graded collecting points. An electrical vibrator of adjustable amplitude and frequency

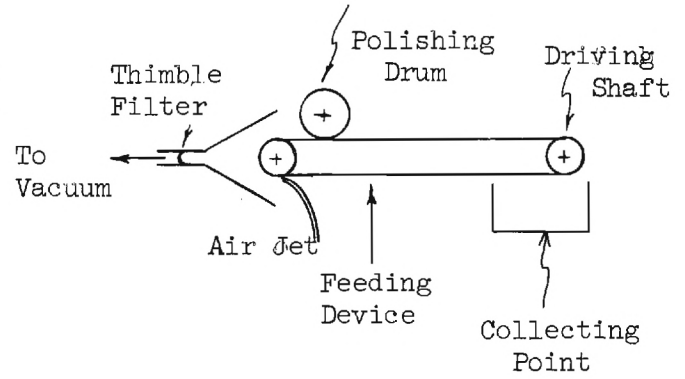
was connected to the lower pulley and was effective in removing the larger adhered particles. A second, mechanically driven eccentric vibrator was applied directly to the moving belt after it passed the lower pulley. This additional and more intense disruptive force removed some of the more strongly adhered particles. An air jet was directed tangentially against the moving belt immediately after passing the mechanical vibrator. The material that was blown off by the air jet was collected by an external vacuum unit and deposited onto a thimble filter. The remaining particles were removed by a lamb's wool polishing drum pressed onto the belt surface. Figure 14(a) is a schematic drawing of method I.

b. Method II. A modification of the above method was made wherein the continuous belt was slowly rotated about two pulleys mounted with their axes horizontal and in the same horizontal plane. Specially constructed feed devices were used to disperse the powder to be classified and to apply it to the belt. The powder was fed downward onto the upper outside of the belt or upward onto the lower outside of the belt. An air jet was used to blow off the larger particles which were then collected by vacuum filtration and the fine material still adhering to the belt was removed by a lamb's wool polishing drum. A schematic drawing of this method is shown in Figure 14(b).

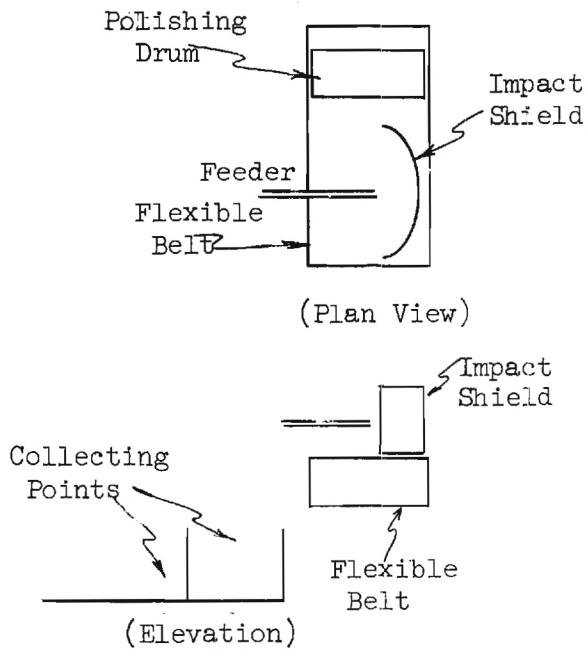
c. Method III. A second modification of the basic design attempted to utilize the bouncing characteristics of the particles as an additional classifying mechanism. In this system, the powder to be classified was directed onto either a flat or concave impact plate mounted above and behind the long axis of the moving belt. A 1/16 inch diameter



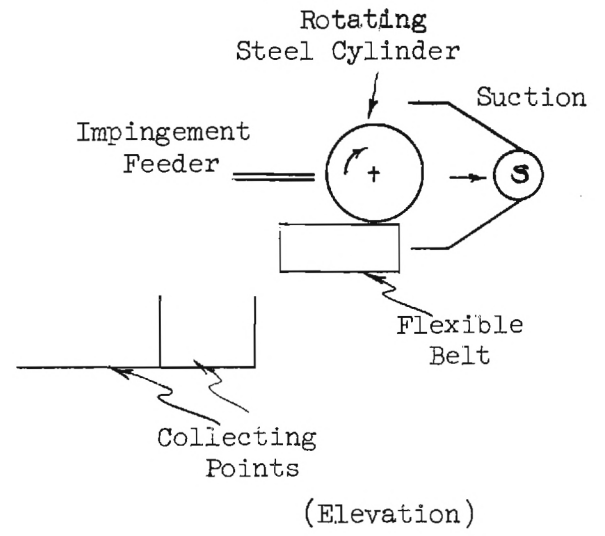
(a)



(b)



(c)



(d)

Figure 14. Flexible Belt Designs.

capillary tube was used as a feeding device in an attempt to get good particle deagglomeration before impaction. Many of the finer particles adhered to the impact plate; the coarsest particles generally rebounded past the surface of the belt and were collected. The intermediate size particles rebounding from the impact plate onto the moving belt surface were subjected to the same classifying procedure as method II. Figure 14(a) is a schematic drawing of this method.

d. Method IV. This modification was essentially the same as method III except, in this case, the powder feed was impacted onto a rotating steel cylinder mounted with its axis horizontal and directly above and parallel to the long axis of the belt. A suction hood was placed directly behind the rotating cylinder to recover those particles that did not adhere to the cylinder or rebound acutely from the surface. Figure 14(d) illustrates this modification.

2. Rotating and Stationary Cylinder Designs

The second basic design attempted to utilize the trajectories of rebounding particles as a classifying mechanism and consisted essentially of a steel cylinder rotating about a vertical shaft. The powder to be classified was impacted onto the rotating surface through a 1/16 inch or 1/32 inch diameter capillary tube placed at a variable distance from the cylinder. With this feeding device, most of the powders were effectively deagglomerated before impaction. The smaller sized particles of the powder adhered to the rotating cylinder and were removed by wiping. The remaining particles either rebounded from or did not strike the surface. The larger particles were collected some considerable distance

away and intermediate ones close to the impact point. This design is shown in Figure 15.

A further modification consisted of a stationary cylinder constructed of brass shim stock onto which the aerosol feed was impacted. Collecting points in the form of concentric cylinders were placed at varying distances from the impact point. This design is shown in Figure 15.

3. Rotating Disk Designs

The third design combined desirable features of both the first two; in it, particles were fed upward through a specially constructed feeding device onto the underside of a disk rotating slowly about a vertical axis. The largest particles rebounded directly into an inner chamber of the feeding device and the intermediate sized particles into an outer chamber. The very fine particles that did not impact the disk but followed the fluid streamlines and the finest of the intermediate size particles rebounding from the disk were collected by a suction tube surrounding the inner feed chamber and deposited on a thimble filter. Many of the smaller particles of the feed adhered to the rotating disk. The adhered particles were next subjected to a high velocity air jet which was surrounded by a vacuum chamber. The particles removed from the disk by the air jet were collected by the vacuum source and deposited onto a "Staplex" filter. Those particles still adhering to the disk were then completely removed by two wiping pads arranged so that the first pad applied an intermediate pressure on the disk and thus removed most of the particles while the second pad applied a rather high pressure to the disk and completely removed the remaining particles.

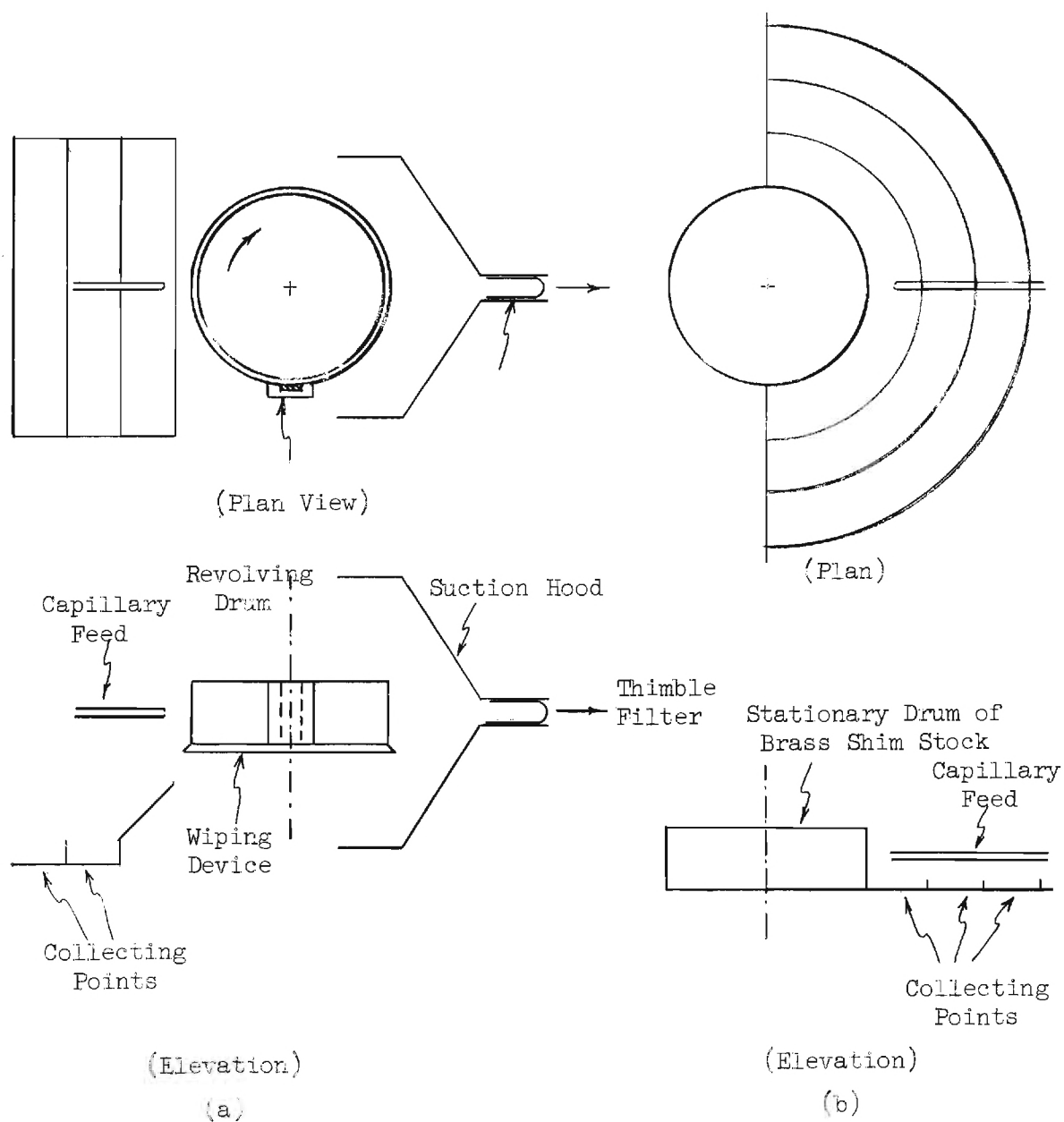


Figure 15. Rotating and Stationary Cylinder Designs.

A modification of the rotating disk system mounted the disk so that its plane was inclined from 10° to 30° off vertical. The powder to be classified was placed in a narrow trough enclosing approximately the lower quarter of the disk, and as the disk was rotated slowly, the smaller particles in the powder adhered to the disk. The adhered material was subjected to a vibratory force just before the uppermost point of the disk travel. The powder that still adhered to the disk was removed by a wiper. Figure 16 shows both variations of the rotating disk designs and Figure 17 is a photograph of the horizontal disk arrangement.

4. System Components

a. Vibrating Devices. An electrical vibrator of variable amplitude and frequency was used in the flexible belt designs. This vibrator was model V-4 manufactured by the Syntron company. A mechanical vibrator was also used which consisted of an eccentric shaft rotating against the moving belt.

It was found that the use of vibratory forces was relatively ineffective in the removal of adhered particles until very strong forces were used. These strong forces created undesirable stresses and vibration throughout the system, thereby necessitating the use of heavy, strong structures. Consequently, vibrators were felt to be an undesirable means of applying disruptive forces to adhered particles.

b. Wiping Devices. In earlier experiments, a lamb's wool polishing drum was pressed against the moving belt or disk to remove the finest adhered particles. The wool drum was unsatisfactory for materials that adhered strongly, since a firm pressure tended to pull loose fibers of the wool which then contaminated the sample. The presence of the

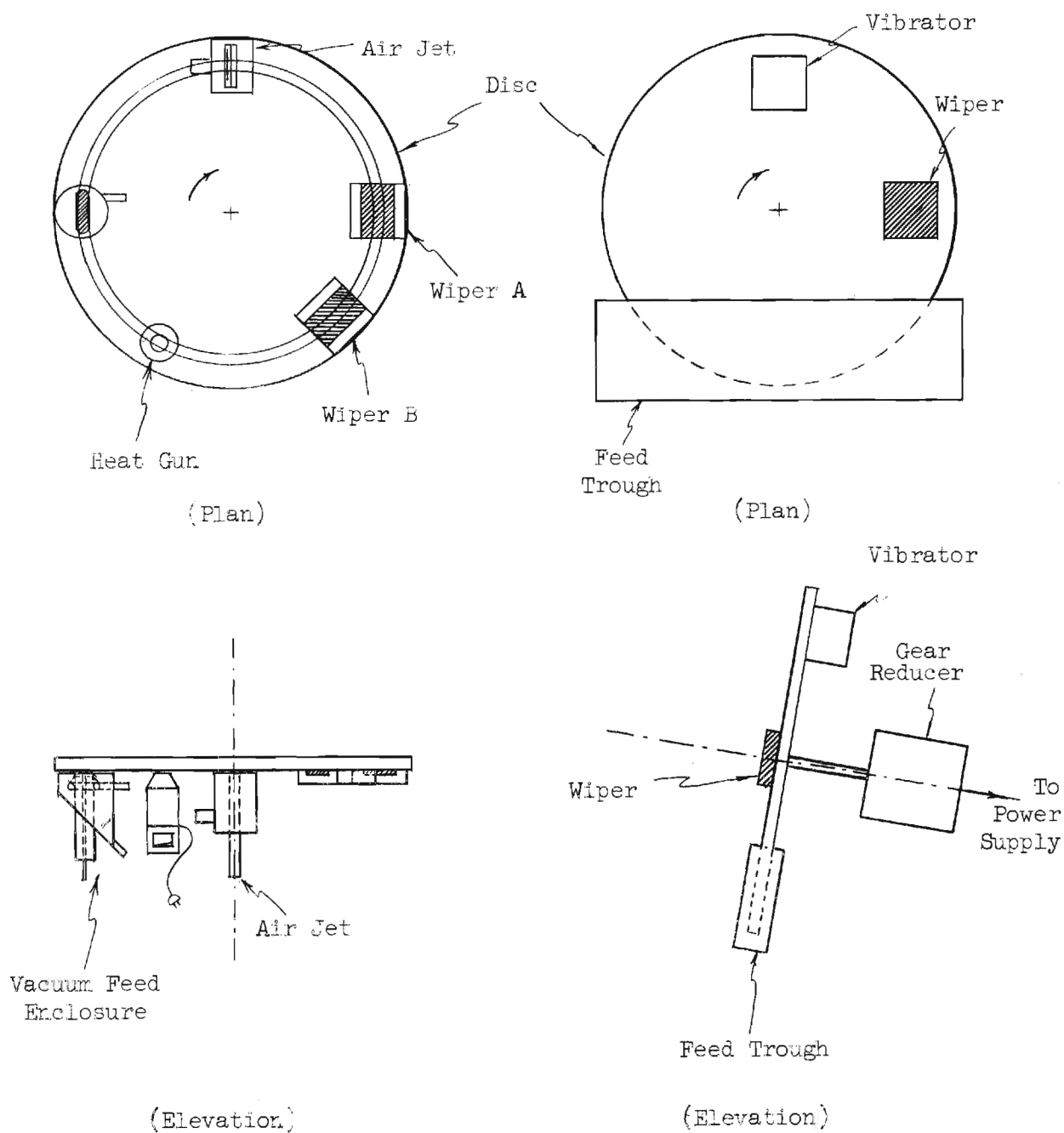


Figure 16. Rotating Disk Designs.

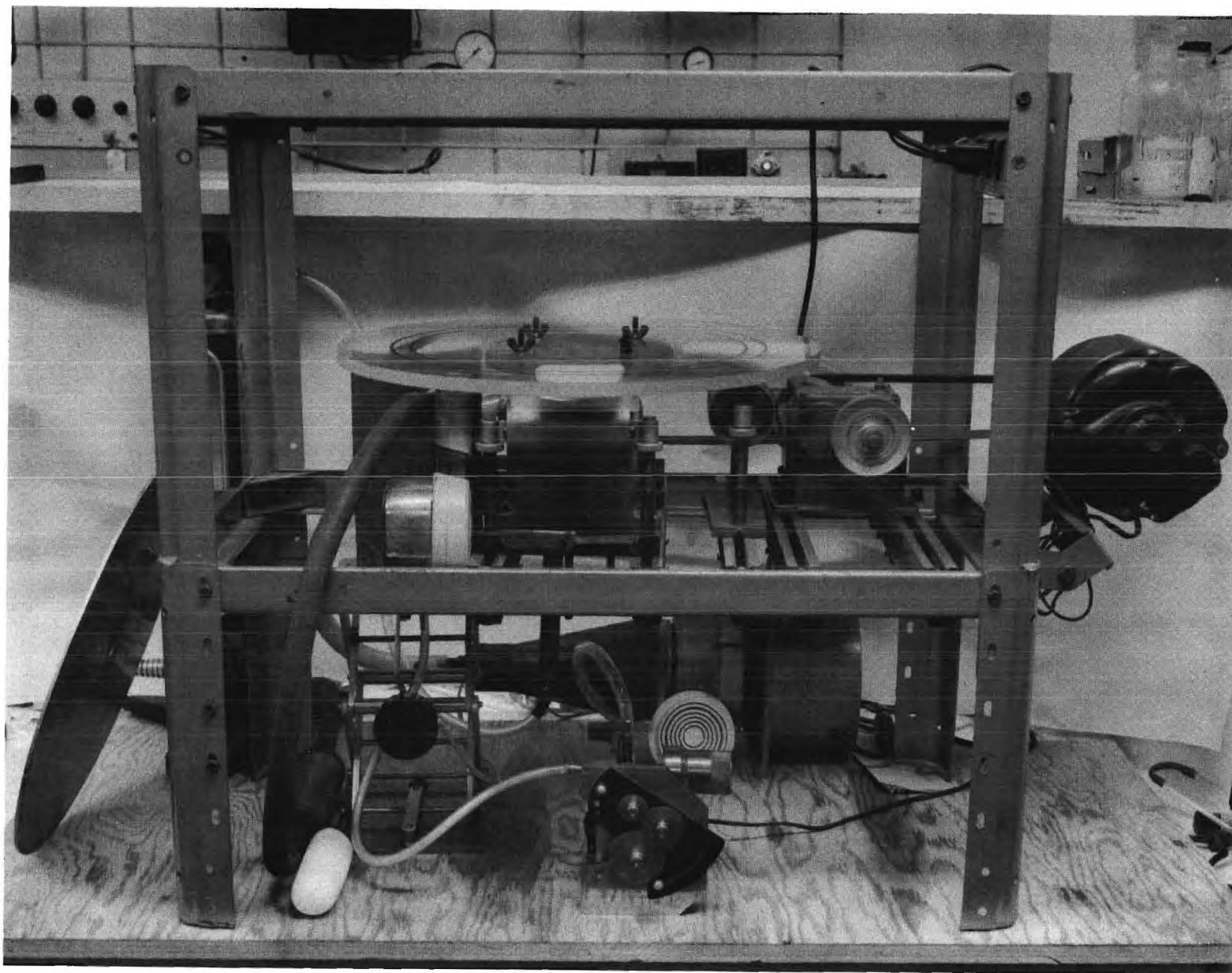


Figure 17. Photograph of Horizontal Rotating Disk Design.

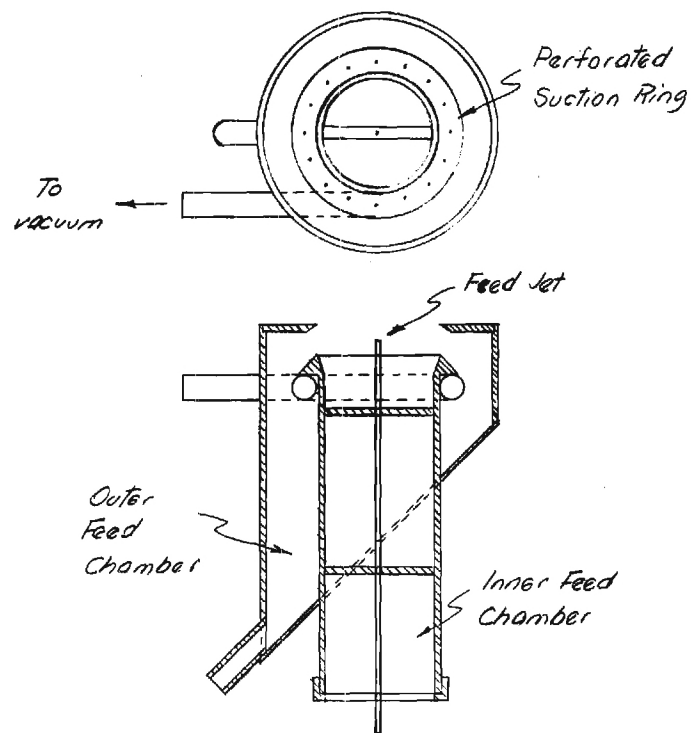
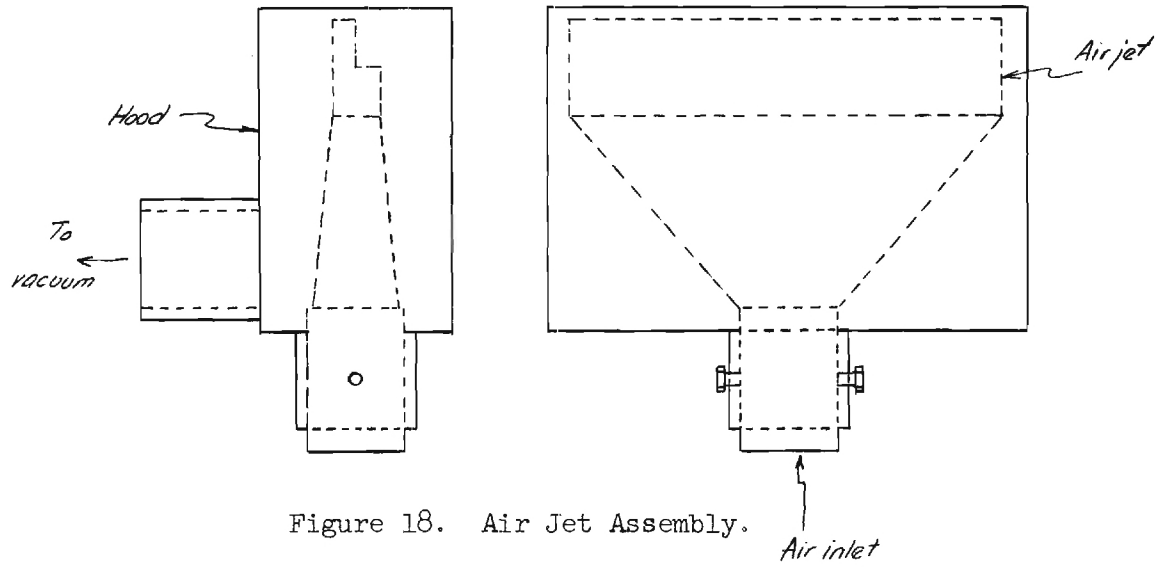
wool fibers caused severe blockages in the operation of the Coulter counter which was used for size analysis of the finest samples.

A later wiping device that proved entirely satisfactory consisted of a plastic holder which pressed a "Kimwipe" or other soft material against the underside of the rotating disk with an adjustable pressure. Cellulose sponges were used in later experiments in place of "Kimwipes" to avoid the slight fiber contamination arising from the tissues.

c. Substrate Materials. Brass shim stock, paper and rubber were used as substrates in the flexible belt designs. It was found that the paper and rubber belts were ineffective as they tended to retain all sizes of the materials very tenaciously, thus making it difficult to remove selectively the sub-sieve particles.

Glass, polished stainless steel, and methyl methacrylate or plexiglass were used as the substrate in the rotating disk method. Glass and plexiglass were very satisfactory from an adhesion standpoint although both showed rather severe erosion from the impinging feed. Polished stainless steel, while excellent from an abrasion standpoint, was not a completely satisfactory material as, in the absence of electrostatic charges, adhesion of particles was very poor.

d. Air Jet Assembly. Air jets used in the flexible belt systems were effective only in dislodging particles from the belt, the material blown off being collected rather inefficiently by a separate external vacuum unit. The air jet assembly used in the rotating disk system was somewhat more refined and is illustrated in Figure 18. The jet itself covered the entire width of powder adhered to the disk and



was of adjustable cross-sectional area. Surrounding the jet and adjacent to the disk surface was a hood connected to a vacuum source. This arrangement minimized powder losses as the volumetric flow rate of air to the jet and the volumetric flow rate of air through the vacuum hood could be balanced to prevent blow-out of powder. The particles blown off by the air jet and collected by the vacuum were deposited onto a "Staplex" filter element.

2. Powder Feed Systems

(1) Feed Jet. Several types of feeding devices were used in an attempt to get good particle dispersion and deagglomeration. The simplest and the most effective device was a 1/16 inch or 1/32 inch diameter stainless steel tube through which the aerosol was blown. The fluid shear in the tube was sufficient to cause deagglomeration of many of the powder aggregates.

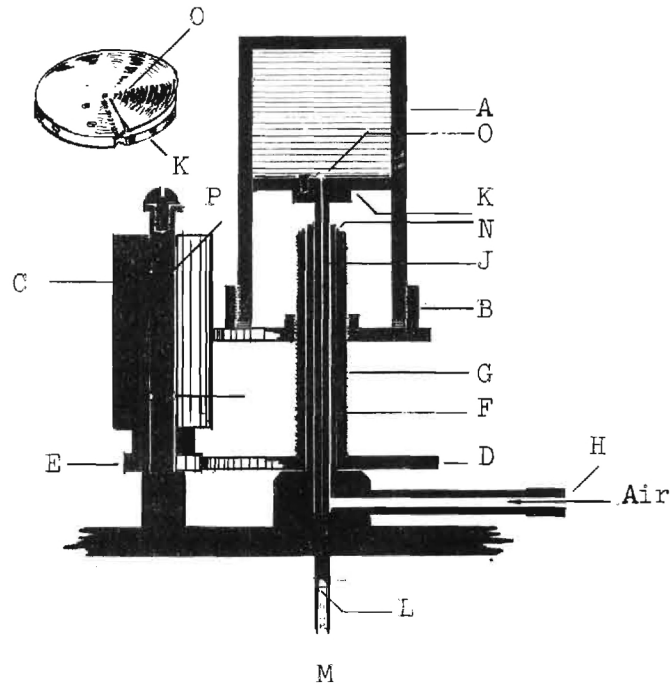
(2) Vacuum Feed Enclosure. Because of the impingement principle it is not possible to impact the smallest particles of an aerosol onto a surface; their inertia is so small as to permit them to follow the fluid streamlines. Thus the smallest particles (generally < one micron) are not impacted onto the moving substrate and some means of recovery is necessary. Early feed enclosure designs surrounded the feed tube with a vacuum chamber to collect those particles that rebounded from the disk and those that were small enough to follow the fluid streamlines and not impact the disk. A further refinement of this design that was used exclusively with the rotating disk system is illustrated on the previous page in Figure 19. With this arrangement, the powder impinges

from the stainless steel tubing onto the rotating disk surface. The largest particles rebound directly from the disk and are collected in the inner chamber. The intermediate particles that rebound from the plate are diverted to the outer chamber by suction applied through a perforated tube surrounding the outer chamber. The largest particles diverted to the outer chamber have sufficient inertia to continue their trajectories past the vacuum source and are collected on the sloping bottom of the outer chamber. The smallest of the intermediate size rebounding particles and those particles too small to impact the disk follow the fluid streamlines to the vacuum source and are deposited onto a thimble filter. Three additional size fractions are thus obtained in addition to those arising from the material adhered to the disk.

(3) Aerosol Generator. The "Wright Dust Feed Mechanism" proved to be the most dependable way in which a well dispersed aerosol cloud could be delivered to the capillary feed tube. The principle on which this apparatus works is illustrated in the schematic diagram of Figure 20.

The powder to be dispersed is contained in the cylindrical container (A) into which it is tightly packed. For best results, the powder should be clean and very dry and predominately less than 50 microns in diameter. When these conditions are met, the powder can be packed into a stable cake, and yet when a thin layer of powder is scraped off the surface, it can be readily redispersed.

The powder is scraped into a groove in the surface of a scraper head (K) and along this groove a stream of dry air or nitrogen is passed so



- A. Dust container
- B. Cap
- C. Long pinion
- D. Gear on threaded spindle
- E. Small pinion
- F. Threaded spindle
- G. Main spindle
- H. Air inlet
- J. Dust tube
- K. Scraper bead
- N. Spring ring
- O. Scraper blade
- P. Spring clips

Figure 20. The Wright Dust Feed Mechanism.

the powder is carried down the inner tube (J). At (L), the powder passes through a small jet and is impacted against the plate (M) which breaks up any remaining aggregates.

The scraping is carried out by rotating the dust holder (A) around the threaded spindle (F), through the intermediary of the gears (C), (E) and (D), which act as a differential gear and cause the holder to travel very slowly down the threaded spindle (F). In this way an extremely thin layer of dust is scraped off at each revolution of the holder (about 1/50th of an inch).

The mechanism is driven by an electric clock motor through a train of change wheels so that a large range of speeds can be obtained at will.

The dust holder has an internal diameter of 1-1/2 inches, but when very low concentrations are being used this can be reduced to half an inch by means of a liner, a smaller scraper head being fitted.

C. Experimental Results

1. Flexible Belt Designs

Several preliminary experiments with the apparatus of Method I indicated that as good or better classification and better product recovery could be achieved with considerably simplified mechanical designs and further work was directed to the construction and evaluation of other designs.

The classification achieved by method III for a special mixture of glass beads is shown in Figure 21. The specially mixed glass beads were fed through a 1/32 inch stainless steel tube onto the underside of a brass shim belt at a feed pressure of 10 psig and feed rate of 0.2 cfm.

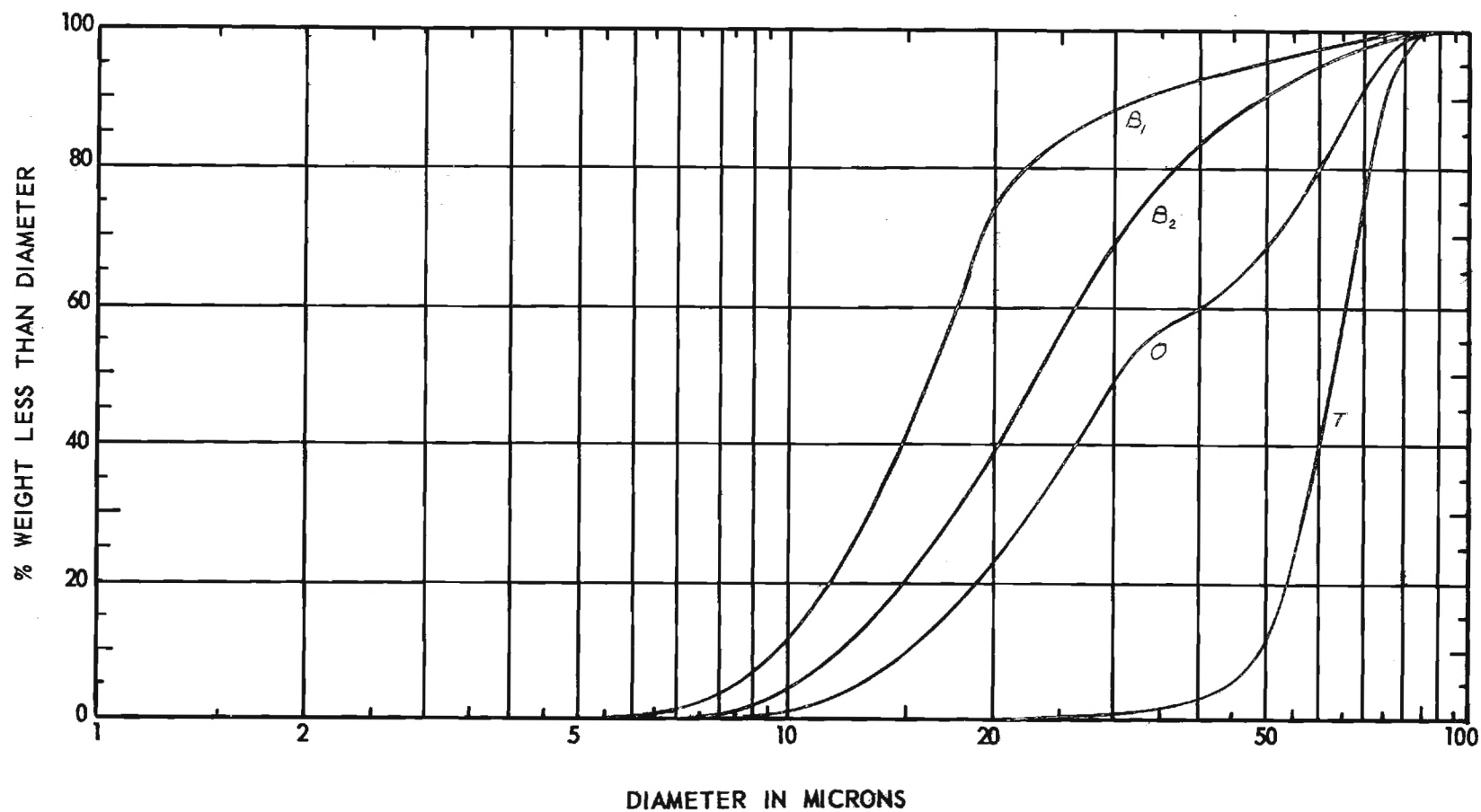


Figure 22. Classification of Glass Beads (Fine) by the Flexible Belt Design (Method II).

The suction hood surrounding the feed jet removed air at 2.5 cfm.

Curve O is the original size distribution of the special mixture of glass beads, curve T is the size distribution of those particles that rebounded from the moving belt and were collected on the bottom of the suction hood, and curves B_1 and B_2 are size distributions of the material that adhered to the belt on two different runs. In run No. 1, the distance from the feed jet to the brass belt was 3 cm and in the second run the distance was reduced to 1.5 cm. Curve B_2 shows poorer separation than does B_1 , probably due to the increased fluid shear resulting in turbulence and poorer impaction efficiency from the nearer feeding point.

Talc powder was also used with method II and the same operating conditions were used as in the preceding experiment except the distance from the feed jet to the brass belt was changed to 1.6 cm. Figure 22 shows the size distributions of the original material, O, the material collected by the feed suction, S, and the material adhered to the plate, B. No size distribution was obtained for the material that rebounded from the belt and collected on the bottom of the suction hood since only a very small fraction of the talc was large enough to overcome the suction applied to the rebounding powder and fall to the bottom.

A second special mixture of glass beads was prepared for use with method II. This mixture was fed downward onto the moving brass belt through a 1/16 inch feed tube at a flow rate of 0.19 cfm. The tip of the feed tube was placed 4 cm from the belt and the suction hood surrounding the feed jet was 0.5 cm from the belt. The air removal rate through the suction hood was 1.10 cfm and air was supplied at approximately

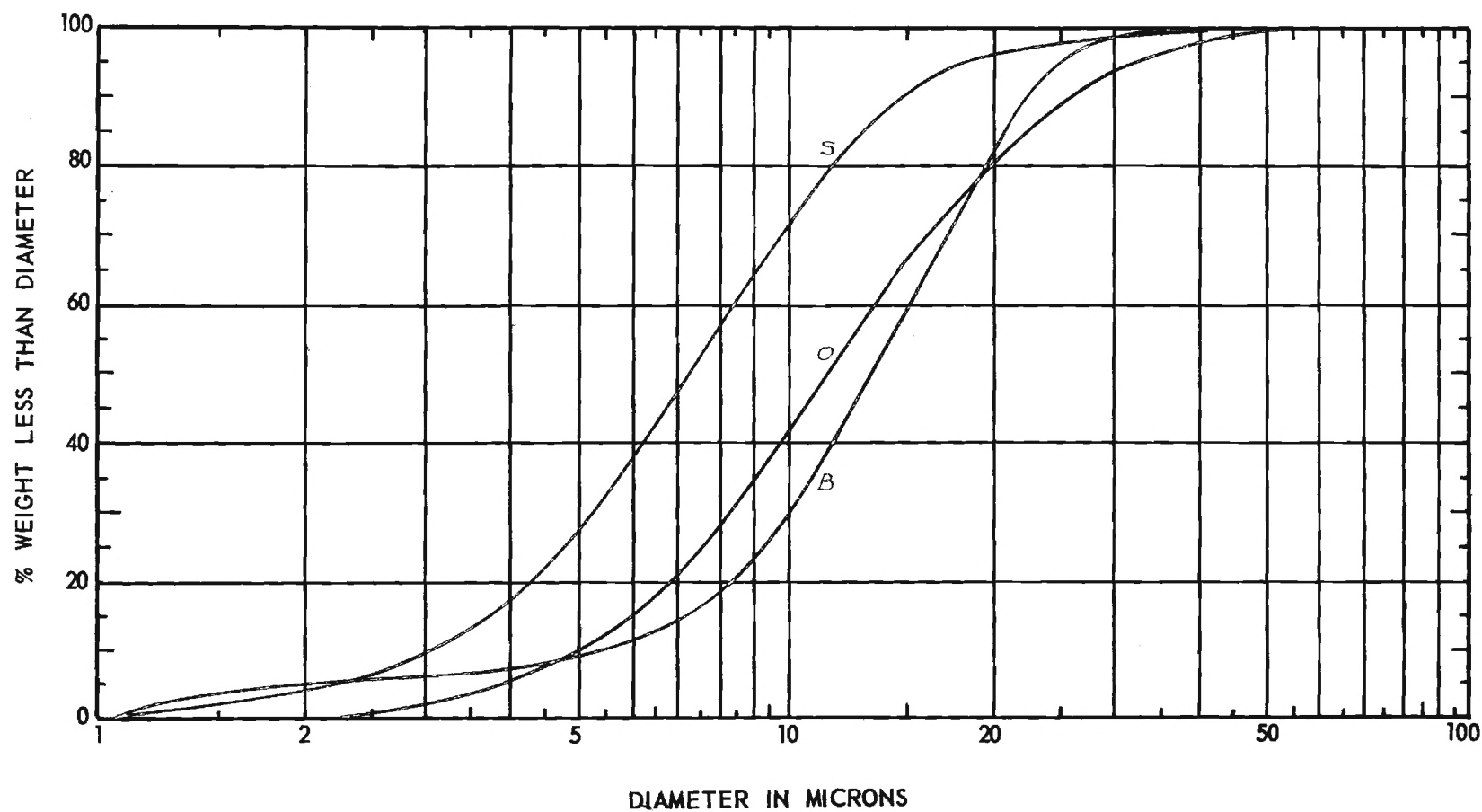


Figure 22. Classification of Talc by the Flexible Belt Design (Method II).

1 cfm to an air jet directed tangentially at the lower side of the belt. An electromagnetic vibrator was placed against the belt at a point just past the feed point. Figure 23 shows the separation achieved with this experiment. Curve O is the original size distribution of the glass beads, curve C is the distribution of those particles removed by the applied vibration, curve J is the distribution of those particles that were blown off the belt by the air jet, curve S is the distribution of the particles collected by the suction hood surrounding the feed jet, and curve B is the distribution of the powder that was removed by the wiper. No significant changes were noted in any of the distributions when the experiment was repeated with no electromagnetic vibration.

The classification resulting from method III was also evaluated with a special mixture of glass beads. The beads were fed through a 1/16 inch tube at 12 psig and 0.25 cfm onto a concave 0.005 inch thick brass shim impact plate placed at the back side of the moving belt and 1/2 inch away from the feed point. Figure 24 shows the classification achieved with the system. Curve O is the original size distribution of the glass beads, curve P is the distribution of those beads that adhered to the impact plate, curve T is the distribution of those particles that rebounded past the belt, and curve B is the distribution of the material that rebounded onto the belt and adhered. No air jet remover or external vibrator were used in this experiment.

A second modification of method III was evaluated using another special mixture of glass beads. In this experiment, the concave brass impact plate was replaced by a flat, vertical steel plate.

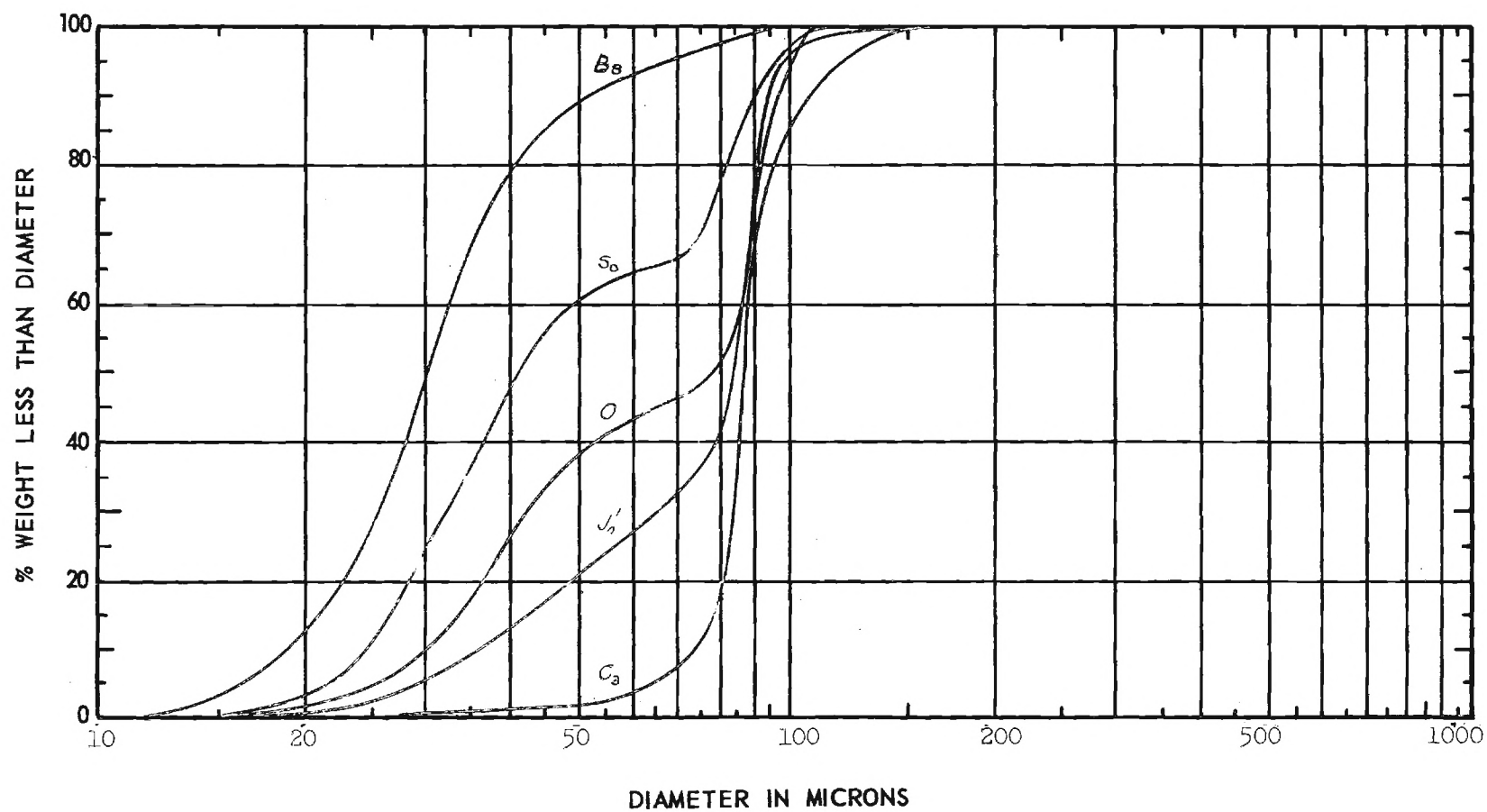


Figure 23. Classification of Glass Beads (Coarse) by the Flexible Belt Design (Method II).

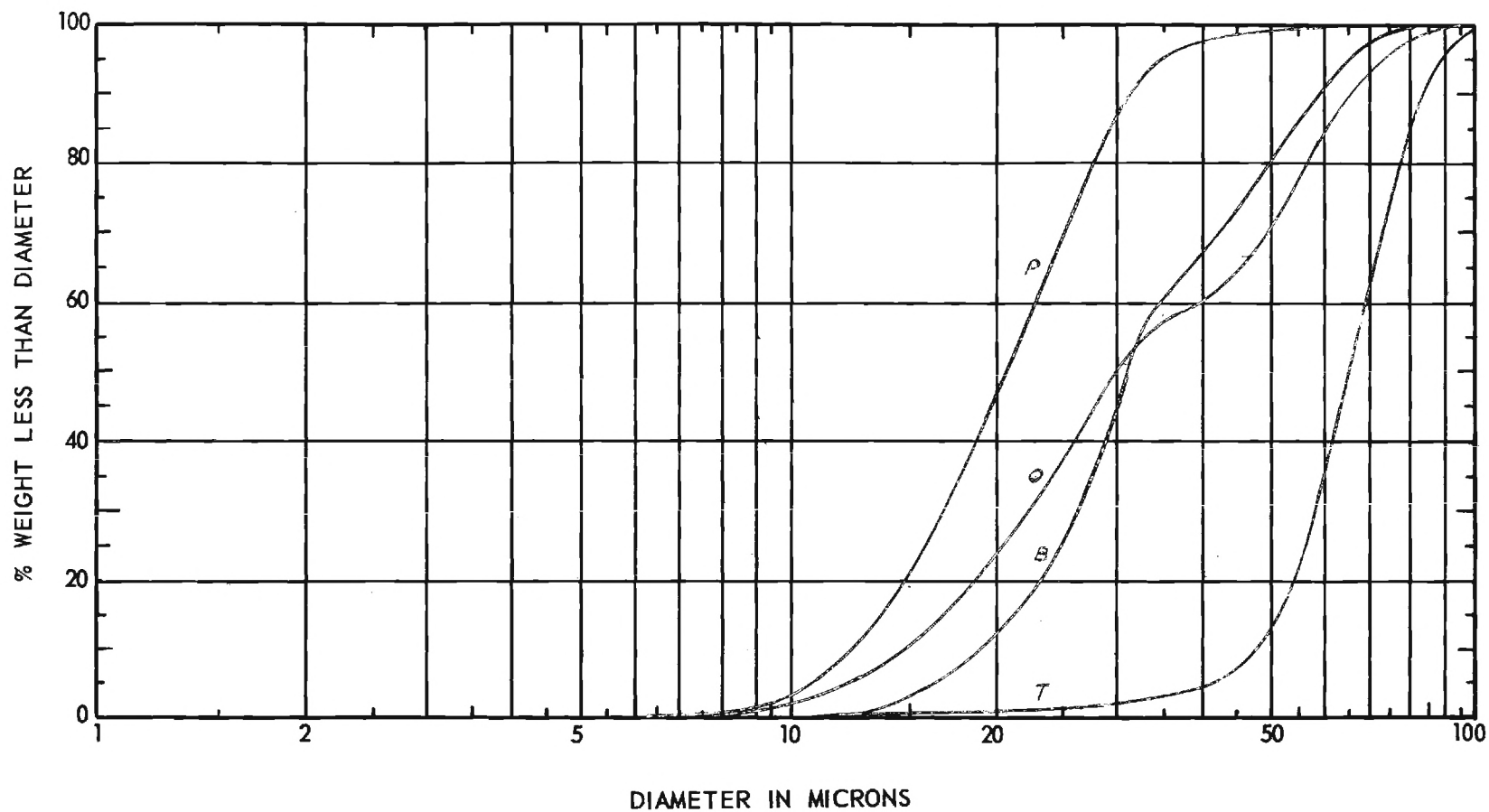


Figure 24. Classification of Glass Beads (Fine) by the Flexible Belt Design (Method III).

The classification resulting from this modification is shown in Figure 25.

The classification by method IV was evaluated using a mixture of glass beads impacted onto a slowly rotating steel cylinder through a 1/32 inch tube at 12 psig and 0.25 cfm. Figure 26 shows the classification achieved with this system. This experiment was repeated using an applied electromagnetic vibration and an air jet remover. Very few of the particles that adhered to the brass belt were removed by the action of these additional disruptive forces and there were no significant changes in the size distributions of the collected materials.

2. Rotating and Stationary Cylinder Designs

Classification by the rotating cylinder design was evaluated with two special mixtures of glass beads, one having a coarse distribution and the other a considerably finer distribution. The material to be classified was impacted onto a steel cylinder rotating at 4 rpm through a 1/32 inch tube at 10 psig and 0.20 cfm.

For the coarser original distribution of glass beads, only the finest and coarsest fractions were analyzed. These results are presented in Figure 27 where curve B is the distribution of those particles that adhered to the cylinder and curve Q is the distribution of those particles that rebounded from the cylinder.

The classification of the finer original distribution of powders is shown in Figure 28 where curve B is the distribution of particles that adhered to the cylinder, curve Q is the distribution of particles that rebounded from the cylinder to the nearest collection point, and curve T

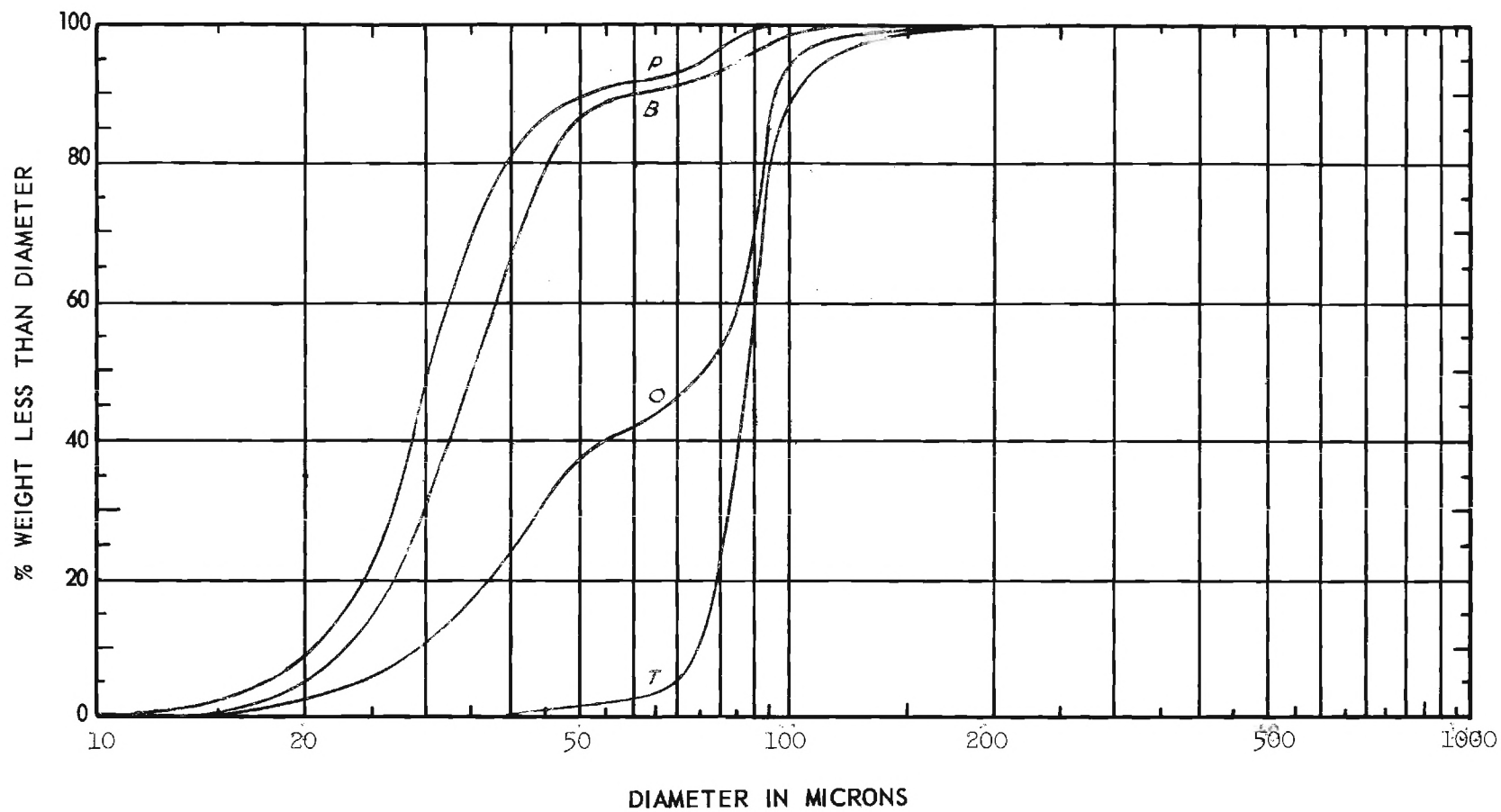


Figure 25. Classification of Glass Beads (Coarse) by the Flexible Belt Design (Method III).

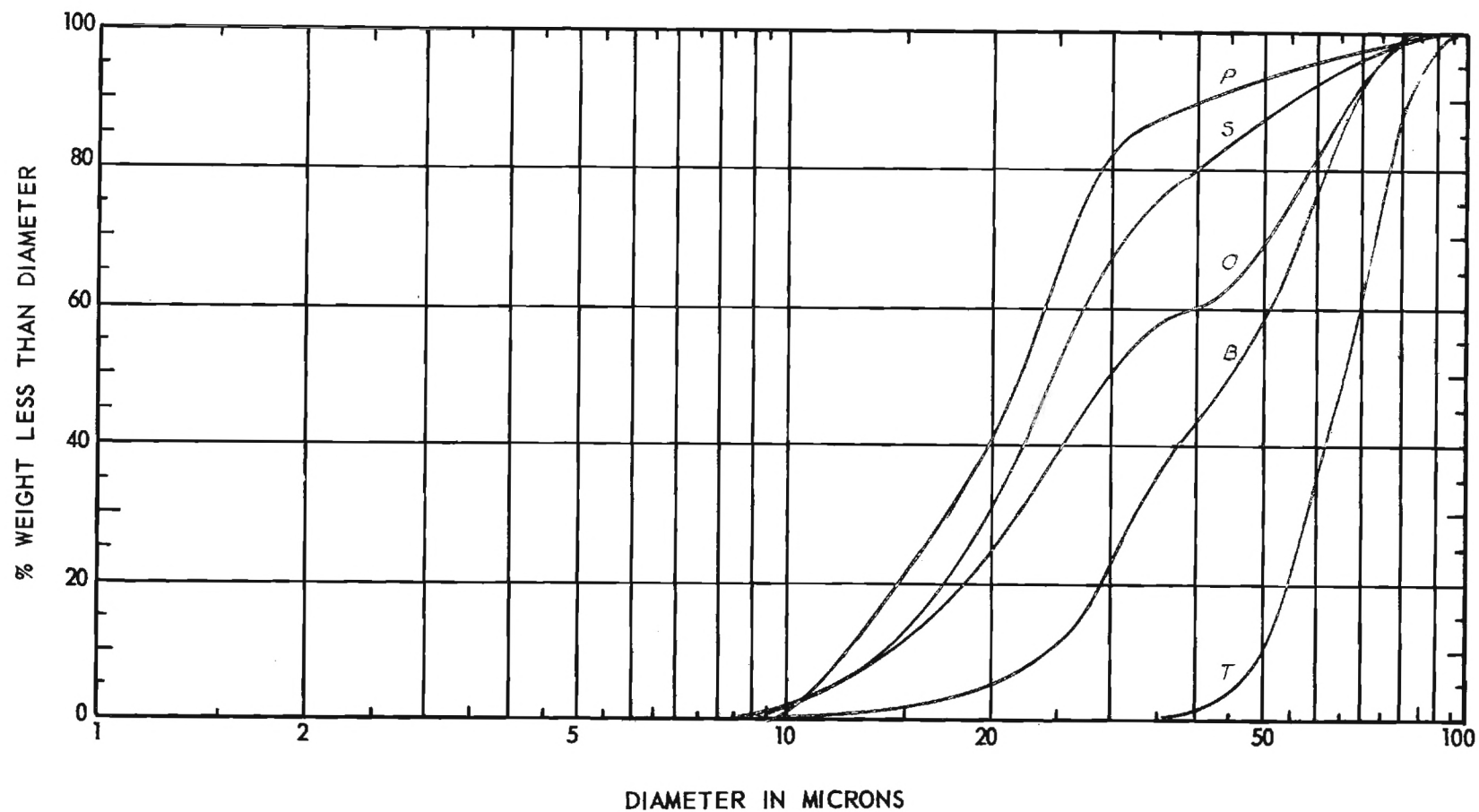


Figure 26. Classification of Glass Beads (Fine) by the Flexible Belt Design (Method IV).

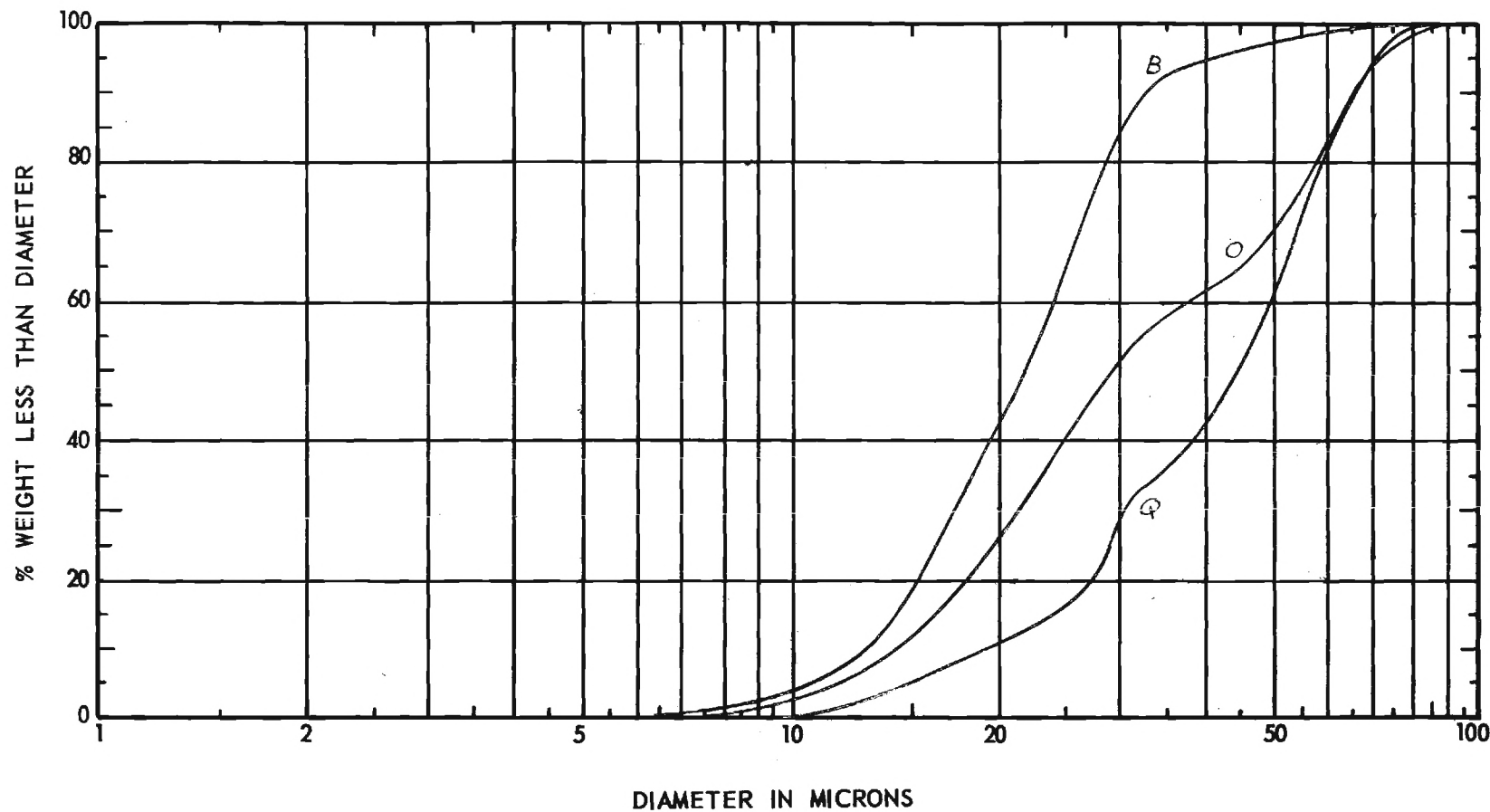


Figure 27. Classification of Glass Beads (Fine) by the Rotating Cylinder Design.

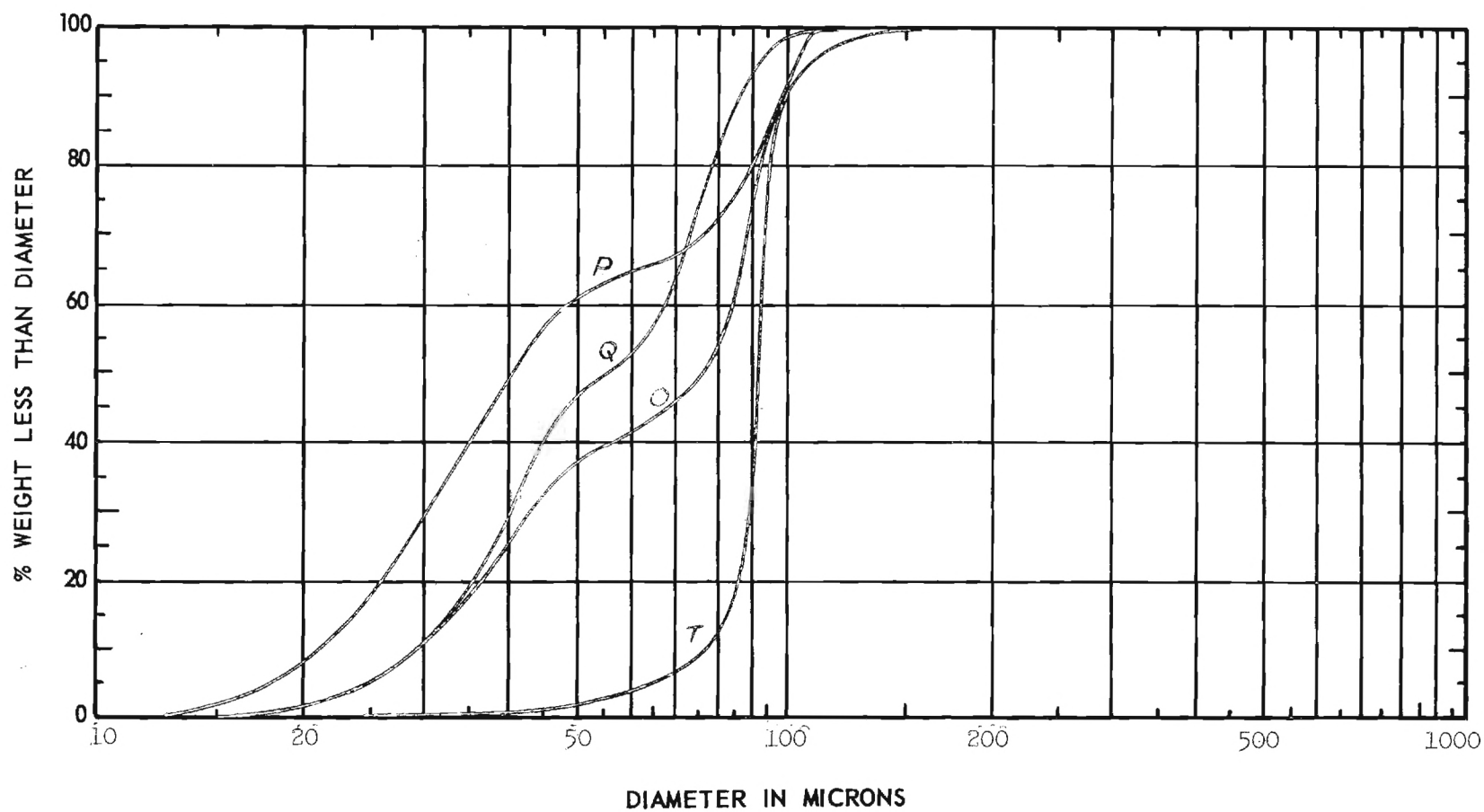


Figure 28. Classification of Glass Beads (Coarse) by the Rotating Cylinder Design.

is the distribution of those particles that rebounded from the cylinder to the farthest collection point. The operating conditions were the same for both runs.

The stationary cylinder design was evaluated by impacting a mixture of glass beads onto a cylinder formed of 0.005 inch brass shim stock through a 1/16 inch tube at 10 psig and 0.19 cfm. The feed tube was placed 2 cm from the cylinder. The classification by this design is shown in Figure 29 where curve P is the distribution of those particles that adhered to the cylinder, curve Q is the distribution of rebounded particles that were collected in the nearest collection point, curve R is the distribution of particles collected at an intermediate distance, and curve T is the distribution of those particles that rebounded farthest from the cylinder. The size distribution of the original mixture of glass beads was the same as the distribution of the sample R within the limits of experimental error.

3. Rotating Disk Design

a. Horizontal Disk. This design was extensively evaluated with a number of powders of widely varying properties. The Wright dust feed was used as the aerosol generator for this design and powder and air flow rates from the generator were regulated for each powder tested so that the powder feed rate was just balanced by the air removal rate of the vacuum feed enclosure. The distance from the end of the feed tube to the disk surface was one inch.

In a typical run, CaCO_3 aerosol was impacted onto a plexiglass disk at 10 psig and a volumetric flow rate of 20 liters per minute with a dust

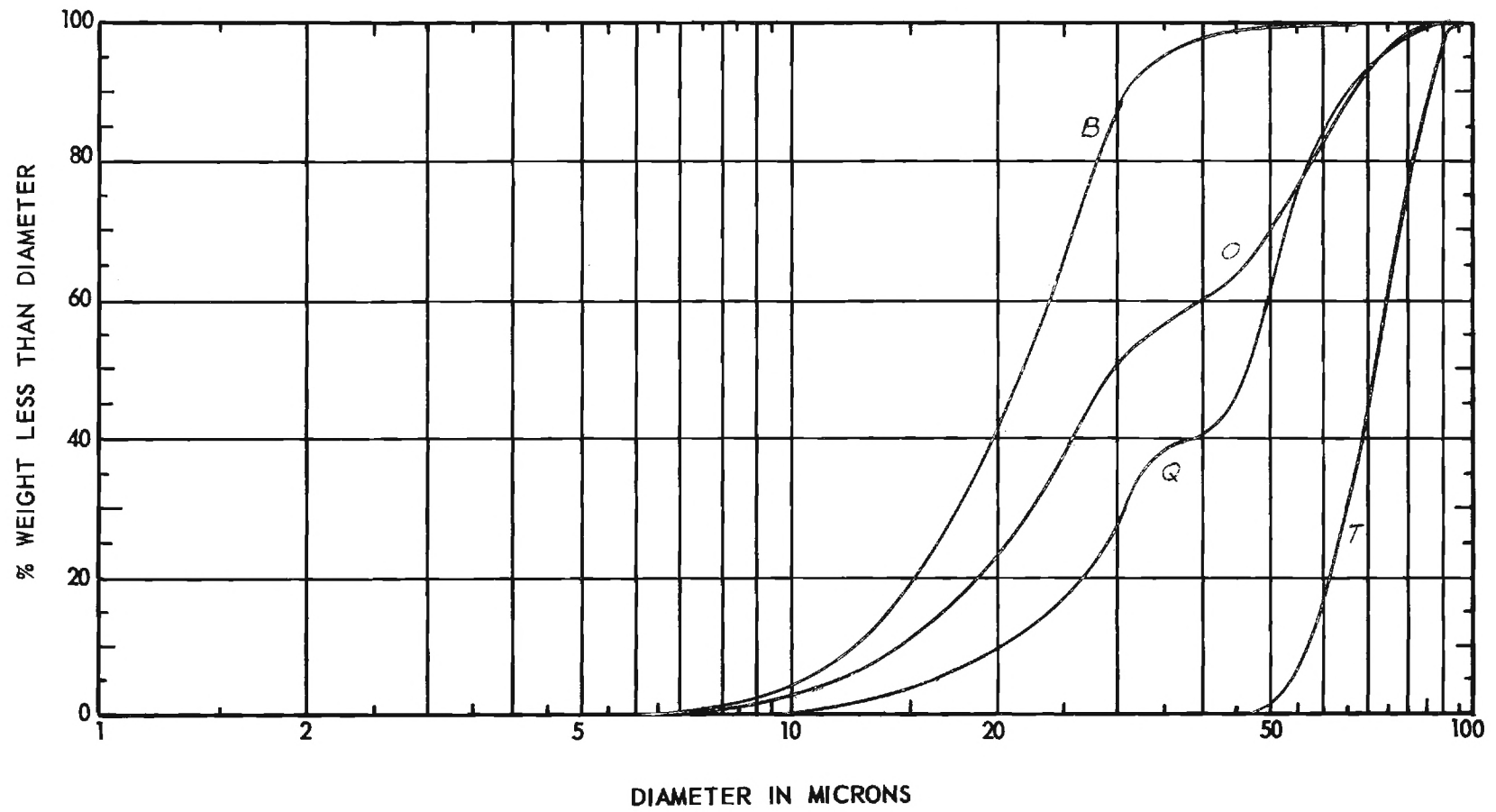


Figure 29. Classification of Glass Beads (Fine) by the Stationary Cylinder Design.

concentration of 0.002 cubic centimeters per liter. Air was removed from the vacuum feed enclosure at a rate sufficient to prevent any blow-out of the dust into the room. Air was supplied to the jet at a volumetric rate of 3 cfm with a resulting jet velocity of approximately 150 meters per second. The air removal rate of the suction hood was sufficient to ensure a negative pressure at the hood periphery, thus removing and depositing onto a filter all particles dislodged by the air jet. Two wiping pads were pressed against the disk to distribute more evenly the pressure on the disk. The second pad was moistened with a liquid to facilitate complete removal of all material adhered to the disk. A heat gun directed warm air onto the disk at a point immediately past the second wiping pad to thoroughly dry the disk before passing again to the feed point.

Figure 30 shows the classification resulting from this run. Curve O is the original distribution, curve T is the distribution of material collected in the inner feed enclosure, curve M is the distribution of material collected in the outer feed enclosure, curve AJ is the distribution of material removed from the disk by the air jet and collected on the "Staplex" filter, curve A is the distribution of material collected on the first wiping pad and curve B is the distribution of material collected on the second wiping pad.

Figures 31 and 32 show the classification achieved by the rotating glass disk for talc and ZrO_2 , under approximately the same experimental conditions as the previous experiment.

Figure 33 shows the classification by particle size of a mixture

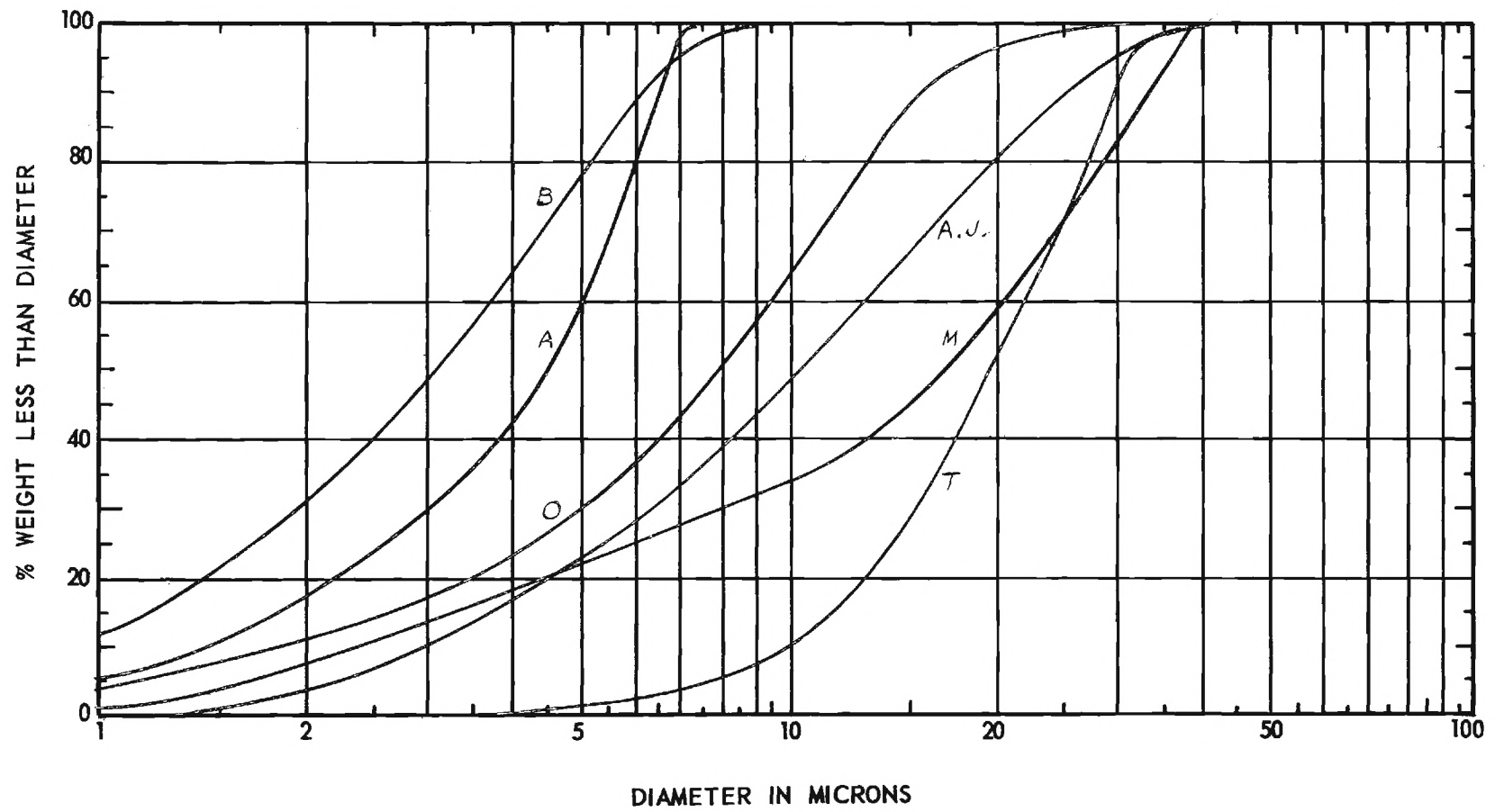


Figure 30. Classification of CaO_3 by the Horizontal Rotating Plexiglass Disk.

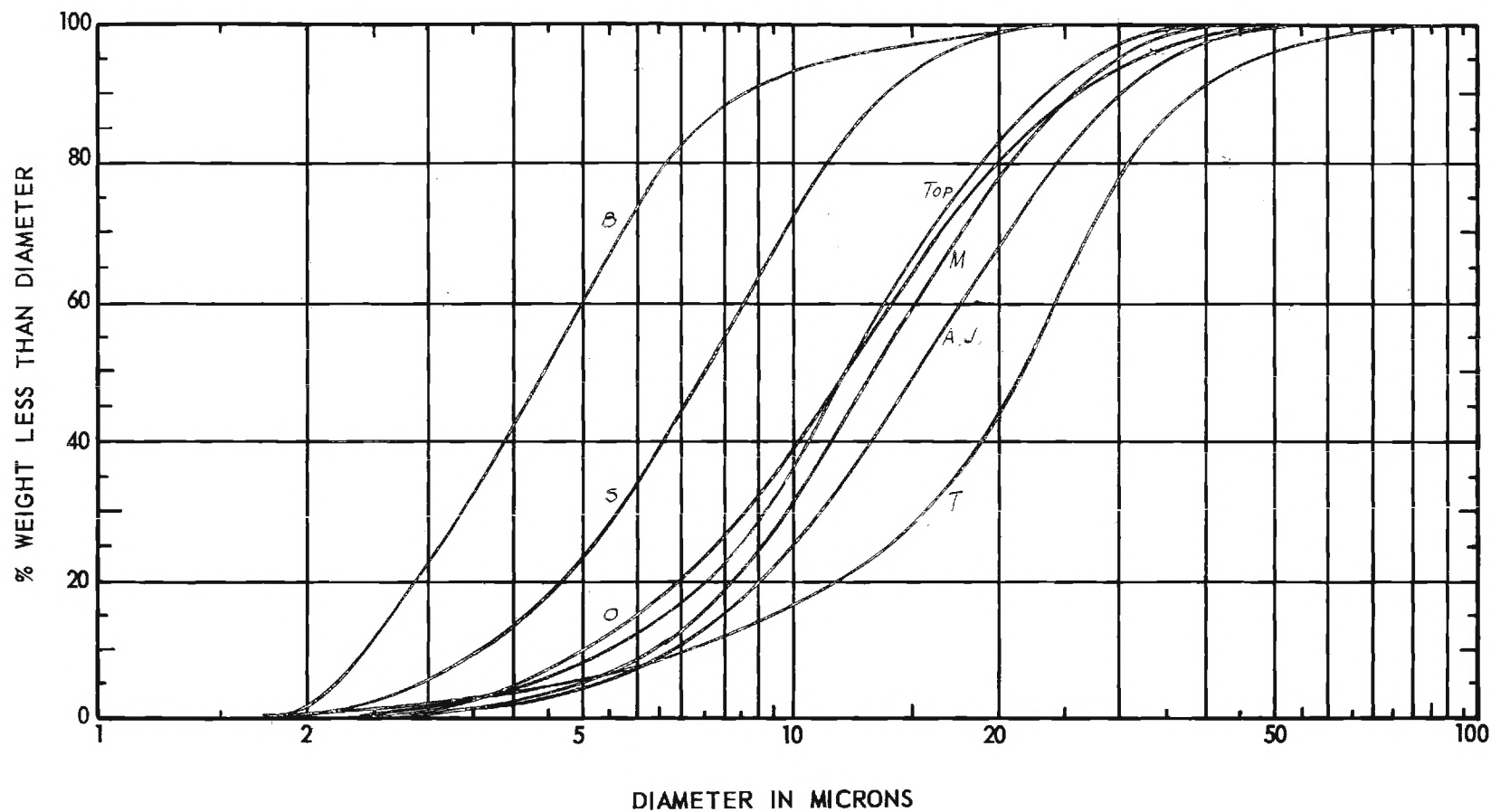


Figure 31. Classification of Talc by the Horizontal Rotating Glass Disk.

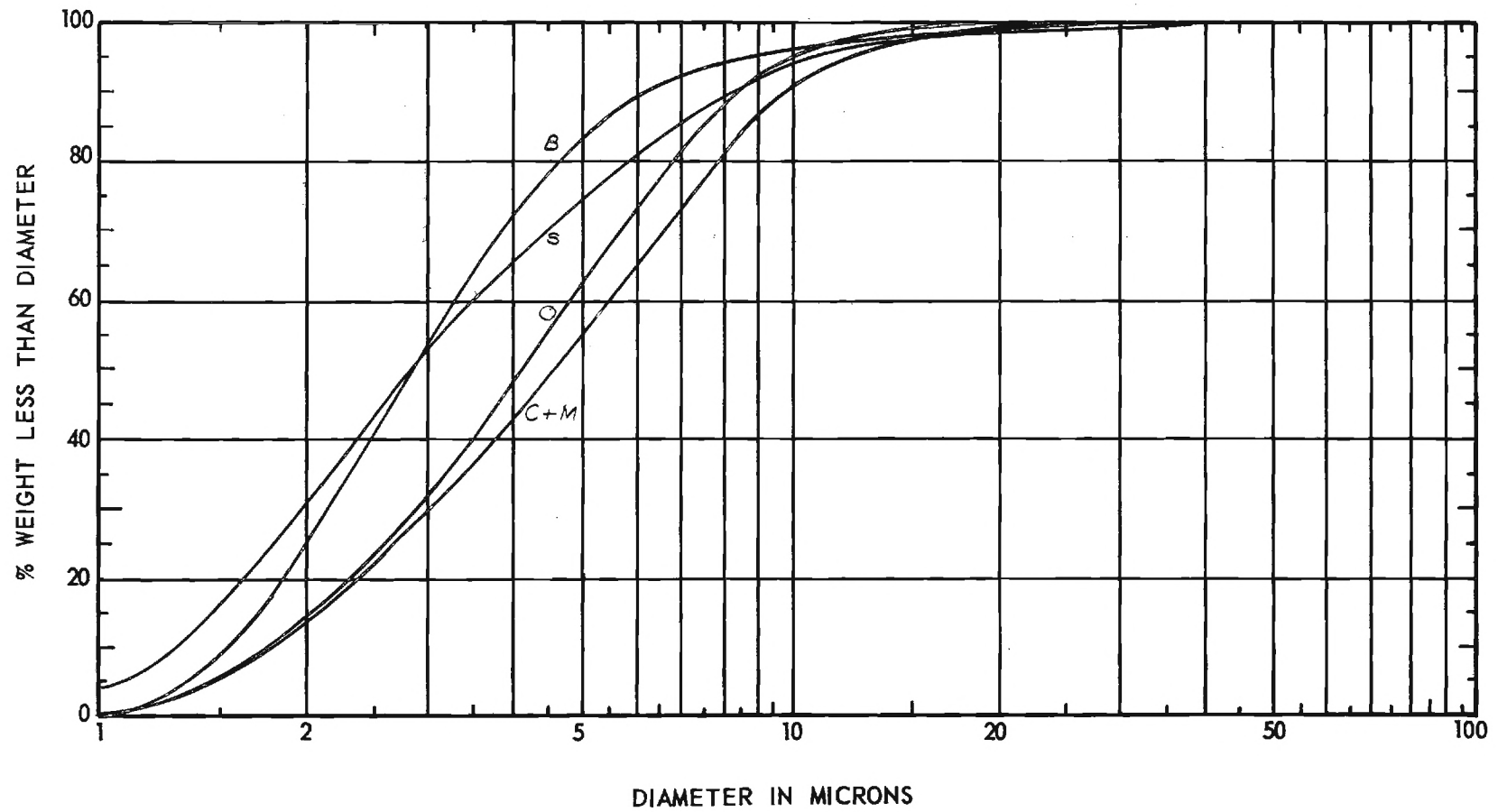


Figure 32. Classification of ZrO₂ by the Horizontal Rotating Glass Disk.

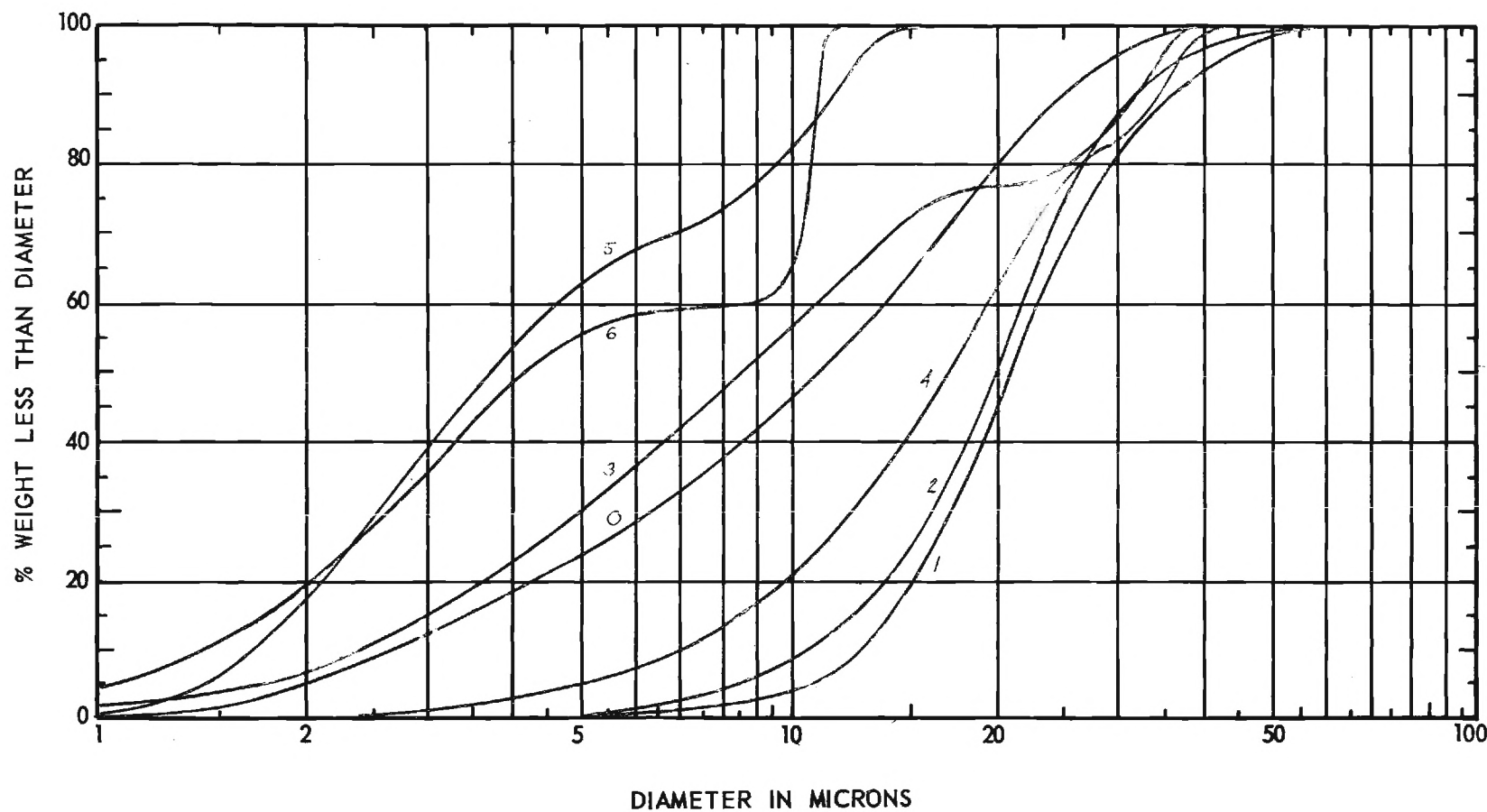


Figure 33. Classification by Size of a NiO-BaSO_4 Mixture by the Horizontal Rotating Plexiglass Disk.⁴

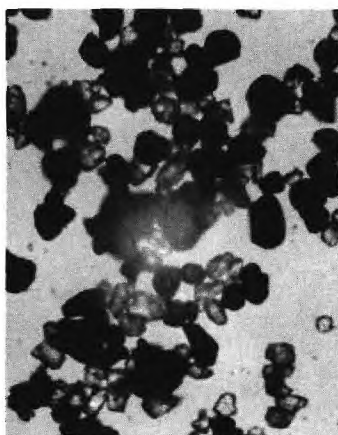
of BaSO_4 and NiO powder and Figure 34 is a series of micrographs of each size fraction showing the separation achieved both by size and physical nature. Table V shows the classification by composition achieved with a plexiglass and a steel rotating disk for an aerosol composed of plastic beads and finely ground NaCl . Analysis was performed by a gravimetric technique in which the per cent soluble material, e.g., NaCl , was determined for each sample.

b. Inclined Disk. Several exploratory experiments with the inclined disk design failed to yield encouraging results. It was hoped that only the finest particles of a mass of particles would adhere to the inclined disk; however, it was found that very few particles adhered to the disk in the absence of any appreciable electrostatic charge and those particles that did adhere were of approximately the same size distribution as the original material. Figure 35 shows the original size distribution of BaSO_4 powder and the distribution of material adhered to the inclined disk.

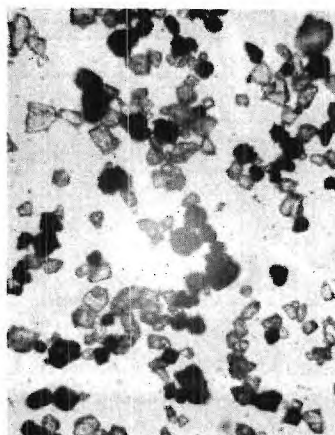
D. Particle Size Analysis

Size fractions collected in this study were analyzed for particle size distribution by the Sharples micromerograph if the mean diameter was above 10 microns diameter and by the Coulter counter if the mean was below this. Microscopic examination of the collected samples was made to determine the approximate size range of each sample.

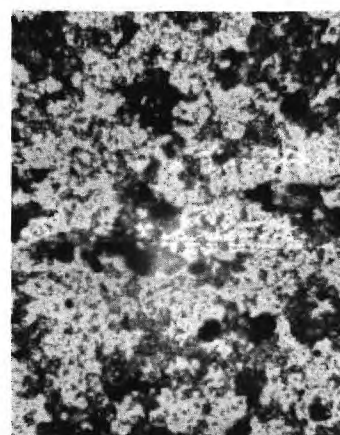
The Sharples micromerograph is an automatic air sedimentation device. This instrument is limited both in the amount of sample required for analysis and in the minimum size to which it is applicable. Many of



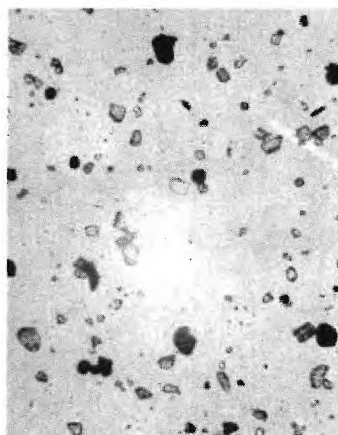
Fraction collected in inner
feed chamber



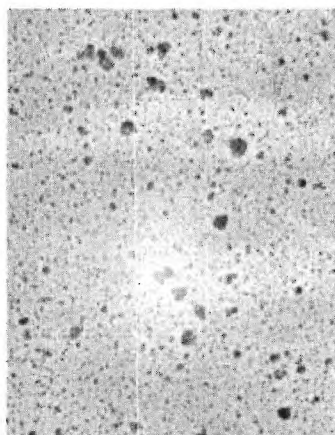
Fraction collected in outer
feed chamber



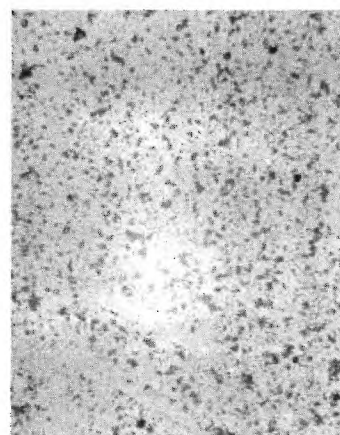
Fraction collected by feed
suction



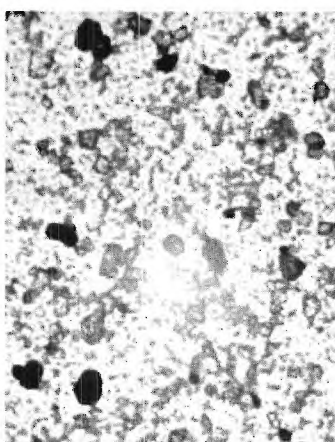
Fraction removed by air jet



Fraction collected at first
wiper



Fraction collected at second
wiper



Original mixture

Figure 34. Micrographs of BaSO_4 -NiO Separation by the Horizontal Rotating Plexiglass Disk (all micrographs 325x).

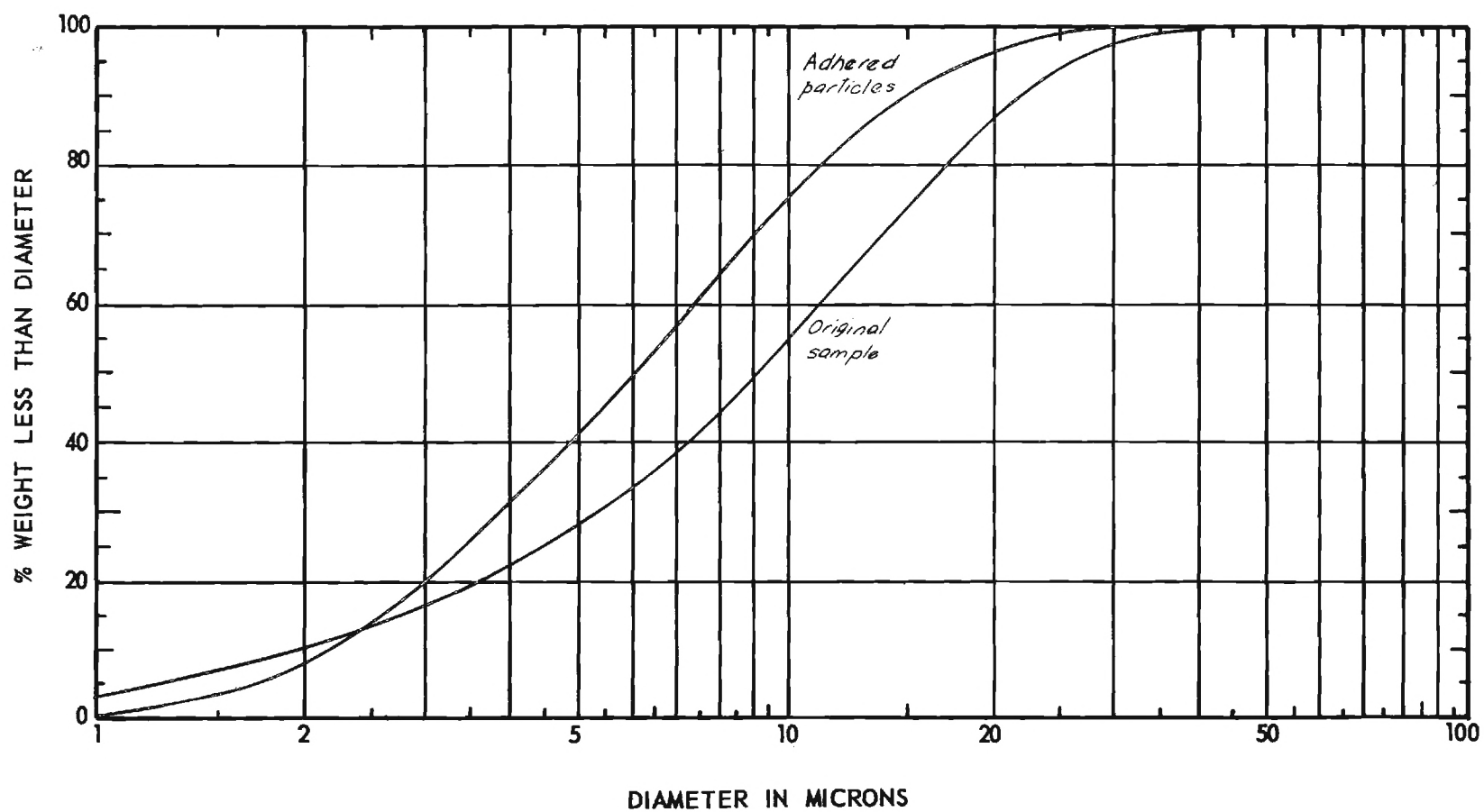


Figure 35. Classification of BaSO_4 by the Plexiglass Inclined Rotating Disk.

TABLE V

SEPARATION OF A NaCl POWDER - PLASTIC* BEADS MIXTURE
BY THE HORIZONTAL ROTATING DISK

Sample Identification	Stainless Steel Disk		Plexiglass Disk	
	% NaCl	% Plastic	% NaCl	% Plastic
Coarse Fraction Collected in Inner Feed Chamber	52	48	31	69
Intermediate Fraction Collected in Outer Feed Chamber	86	14	90	10
Fine Fraction Collected by Feed Suction	21	79	40	60
Fraction Adhered to Disk	99+	1-	70	30
* Original Composition: - 63% NaCl				

the finer fractions collected consisted of only a few milligrams of material, hence the small amount of material available and the poor deagglomeration of this material by the micromerograph necessitated a more sensitive method of analysis for the smaller size ranges. The Coulter counter is an electronic size analysis instrument which measures the volume of each particle and the total number of particles in a given volume of suspension as the liquid suspension flows through a small orifice immersed between two electrodes. This instrument requires only a few milligrams of powder for analysis and is capable of size measurement into the sub-micron range.

The size distributions of soluble materials which were too fine for analysis by the micromerograph were determined by optical microscope count. The distributions of other materials consisting predominantly of particles less than 0.5 micron diameter, e.g., TiO_2 , were determined by electron micrographs.

V. DISCUSSION OF RESULTS

A. General

Examination of the size distribution curves in the previous section, particularly those resulting from the rotating disk design, reveal that continuous size classification devices have been constructed that operate effectively in the normal sub-sieve range. The horizontal rotating disk design was found to be the most efficient design both from the standpoint of product recovery and the actual classification achieved. This design was tested with powders having spherical particles (glass and plastic beads from 6 to 70 microns in diameter) and irregular particles (talc, BaSO_4 , TiO_2 , CaCO_3 , NiO , NaCl , and Y_2O_3 from 100 microns to sub-micron diameters). Good classification was achieved in every case with the mass median size of the finest fraction generally ranging from 2 to 5 microns diameter.

Comparison of the size distributions of the finest and the coarsest fraction of the CaCO_3 sample shown in Figure 17 indicates a separation efficiency of practically 100 per cent based on these two extremes and a cut size of 10 microns diameter. The finest fraction contains essentially no particles larger than 10 microns diameter while the coarse fraction has greater than 90 per cent by weight of its particles larger than 10 microns diameter. The same approximate separation efficiency by size is shown by the NiO-BaSO_4 results presented in Figure 33. Other materials such as talc, ZrO_2 and Y_2O_3 with particles very irregular in shape did not classify as well as the previous two examples although relatively good separation was also achieved with these materials. These results may

be explained in part by the effect of particle shape on the adhesive force in the high humidity environments used in experiments and by the unpredictable rebounding characteristics of irregular particles.

B. Effects of Varying Humidity and Particle Contact Area on the Force of Adhesion Between a Particle and a Solid Surface

It is generally agreed and has been experimentally observed^{14,15} that the adhesive force between a particle and a surface increases as the surrounding relative humidity increases. However, examination of the usual expression of the adhesive force for spherical particles does not show this tendency.

$$F = 4\pi T R \left[1 - \left(1 - \frac{1}{1 + \frac{r}{R}} \right)^2 \right] \quad (5.1)$$

As the relative humidity increases, the radius of the water film surface becomes larger and the adhesion force as described by equation 5.1 is essentially constant since $r \ll R$, or will slightly decrease as r becomes much larger.

This apparent anomaly may be explained if it is assumed that the actual contact point of a particle is rather sharp as in the case of the conical apex shape shown in Figure 36. All "plane" surfaces actually consist of many pits and ridges so it is logical to assume that the actual particle contact is similar to that shown in Figure 36 rather than the idealized concept of a sphere on a perfectly plane surface. The force

14. M. C. Kordecki et al., op. cit.

15. B. Deryagin et al., op. cit.

of adhesion may then be shown by the following equations to increase with increasing humidity and a corresponding increase in the radius of the water film surface.

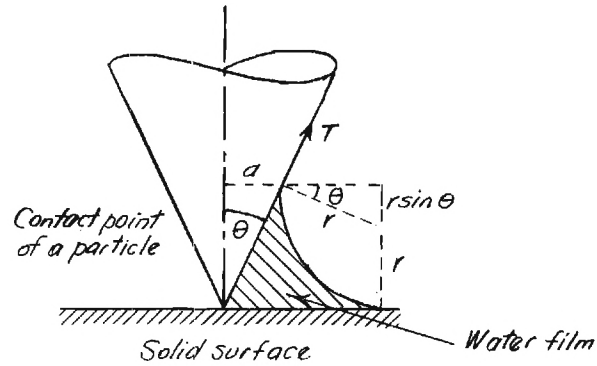


Figure 36. Contact Area between a Conical Particle and a Horizontal Surface.

$$a = r (1 + \sin \theta) \tan \theta \quad (5.2)$$

$$\begin{aligned} F_1 &= \pi a^2 \frac{T}{r} = \pi r^2 (1 + \sin \theta)^2 (\tan^2 \theta) \frac{T}{r} \\ &= \pi T r (1 + \sin \theta)^2 \tan^2 \theta \quad (5.3) \\ &\quad \text{(the force by negative pressure)} \end{aligned}$$

$$\begin{aligned} F_2 &= 2\pi a T \cos \theta \\ &= 2\pi T r (1 + \sin \theta) \tan \theta \cos \theta \\ &= 2\pi T r (1 + \sin \theta) \sin \theta \\ &\quad \text{(the force by surface tension)} \end{aligned}$$

$$F = F_1 + F_2 = \pi T r (1 + \sin \theta) \left[(1 + \sin \theta) \tan^2 \theta + 2 \sin \theta \right] \quad (5.5)$$

Examination of equation 5.5 shows a linear relationship between adhesive force and water film radius. The actual case is probably intermediate between the two extremes presented as would be inferred from examination of Figure 37, which is a plot of the adhesion of spheres on a "plane" surface as a function of humidity.¹⁶

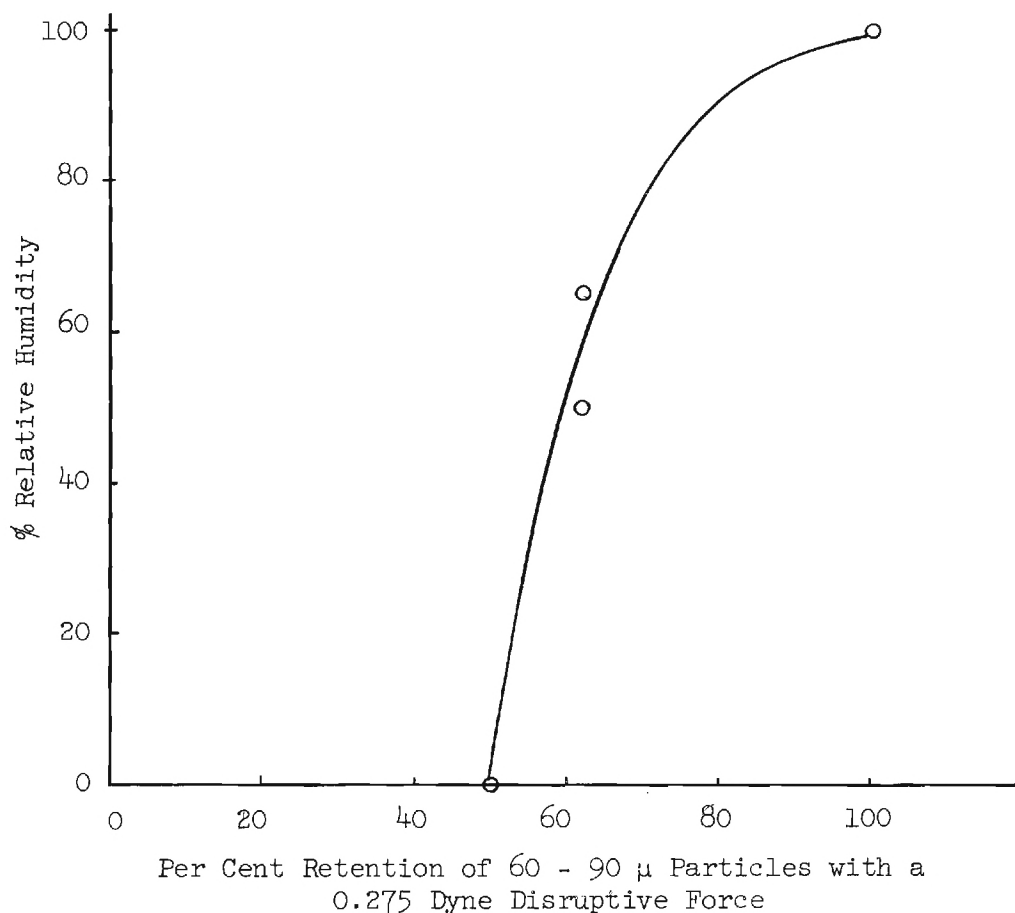


Figure 37. Dependence of Adhesive Force on Relative Humidity.

16. B. V. Deryagin et al., loc. cit.

C. Feed Velocity Effects and Limiting Particles Sizes by Impaction

Upward impact feeding onto a moving surface was found to be the best means of applying a powder to the substrate. In this way, with an applied feed suction, the rebounding characteristics of the particles are utilized as a classifying mechanism in addition to the classification resulting from adhesion. Some experimentation is necessary with each material to be classified by this procedure to determine the optimum feed velocity for minimum substrate erosion yet sufficient velocity to impact the smaller sizes. Most of the classification of the larger particles (from 5 to 100 microns diameter) is a result of their rebounding characteristics from the disk. The finest fraction obtained from those particles adhered to the disk is limited by the smallest sizes that may be impacted onto the disk. The impact factor for a circular jet and a flat plate is defined by the following expression:

$$P = \frac{\rho_s V \delta^2}{18\mu d}$$

or

(5.6)

$$\delta = \sqrt{\frac{18\mu P d}{\rho_s V}}$$

where P is the impact factor (0.15 for flat plate and circular jet), ρ_s is the density of particle, V is the velocity of particle, δ is the particle diameter, μ is the fluid viscosity, and d is the jet diameter. Examination of the above expression indicates that a high velocity jet of small diameter yields the smallest impacted sizes. This knowledge must, however, be tempered by the fact that the optimum velocity for

impaction may result in severe erosion of the substrate and significant particle fracture if a friable material is to be classified. A numerical example of the above expression for TiO_2 powder ($\rho = 3.9 \text{ gm/cm}^3$) in a carrier gas of air ($\mu = 0.00018 \text{ g/cm-sec}$) directed through a 1/32 inch circular jet at 200 meters/sec onto a flat plate gives a minimum impacted particle diameter of approximately 0.25 micron diameter. This suggests that a possible technique for extracting the finest sizes from an aggregate of sizes would be to impact the powder onto a continuously moving surface coated with a sticky material such as oil or a low molecular weight resin. In this way, all particles would be collected on the surface except those particles smaller than the limiting size for impaction.

D. Verification of Theoretical Results

Calculations of the magnitude of adhesive forces acting between objects joined by a film of water have frequently been in considerable disagreement with experimental values. One reason for this lack of agreement may have been due to questionable assumptions as to the curvature of the profile of the water film. The theoretical profiles of water films between plane solid surfaces and horizontal liquid surfaces have been determined in this study with the aid of an analog computer and are presented in an earlier section of this report. Dr. Koichi Iinoya and Mr. S. Asakawa¹⁷ have experimentally confirmed one of these solutions by a photographic technique. Figure 38 shows the theoretical profile between a vertical plane solid and a horizontal liquid surface and between

17. K. Iinoya, Private Communication, Nagoya University, Nagoya, Japan.

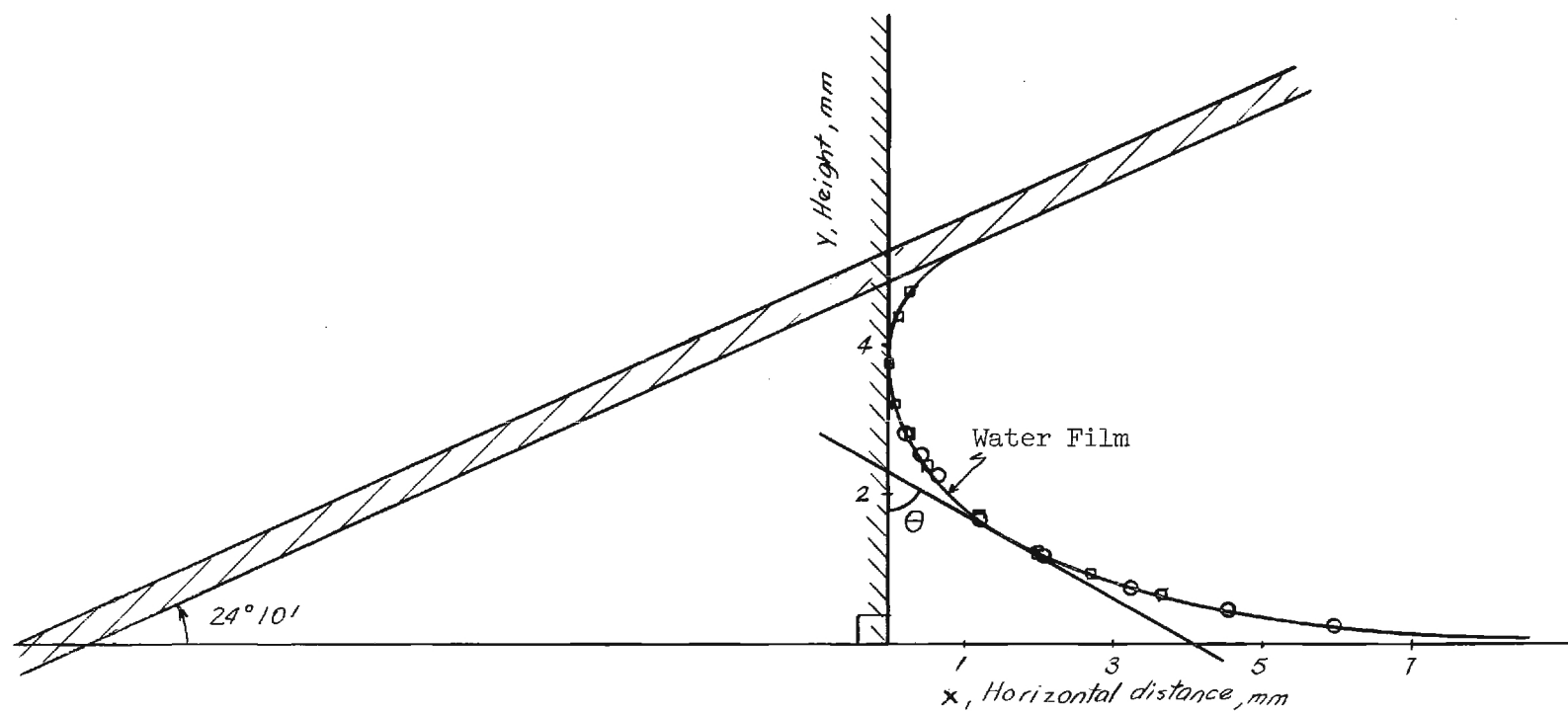


Figure 38. Theoretical and Experimental Liquid Profiles.

an inclined plane surface and a horizontal liquid surface. The points shown on the curve in Figure 38 are the experimental values as determined from the photographs shown in Figure 39. This exceptionally good agreement between theoretical and experimental results tends to confirm the modified methods for force calculation presented in an earlier section and should permit more accurate and reliable force calculations to be made now, especially for large particles (larger than 100 microns diameter) where this effect will be more pronounced. These results may also find use in the development of an improved sintering theory. The curvature of the bridges or "necks" connecting particles in the first stage of sintering is important in determining driving forces for evaporation and condensation or diffusion from these curved surfaces.

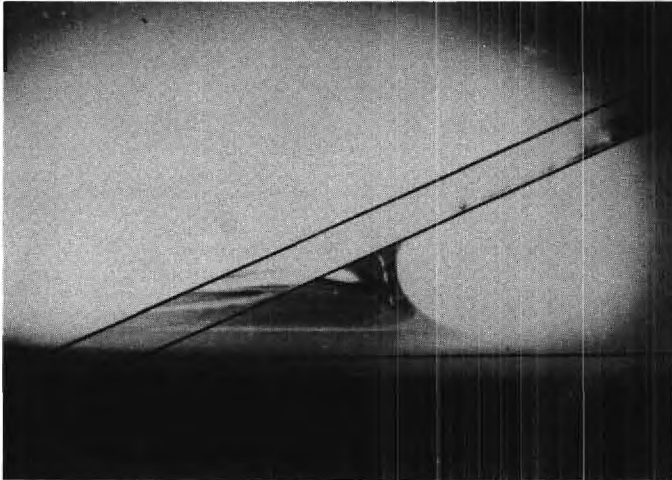
E. Capacity and Recovery Efficiency of Rotating Disk Design

The theoretical capacity of adhered particles by the rotating disk system may be calculated by the following equation if it is assumed that the particles are placed on the surface in a close-packed arrangement in a single layer, and if it is further assumed that the disk is slowly moved so that no unfavorable body or inertial forces are created.

$$G = \left(\frac{\pi}{6} \delta^3 \rho_s \right) \frac{BU}{\delta^2} = \frac{\pi}{6} \rho_s \delta BU \quad (5.7)$$

where G is the theoretical capacity, ρ_s is the particle density, δ is the particle diameter, B is the width of surface, and U is the velocity of surface. As a typical example, let $B = 1$ cm, $U = 5$ cm/sec, $\delta = 20$ microns and $\rho_s = 2.5$ gm/cm³ then,

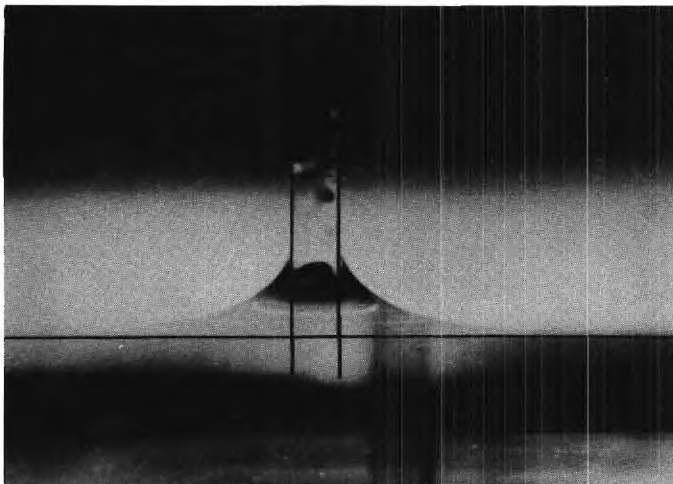
$$G = \left(\frac{\pi}{6} \right) (2.5) (0.002) (300) = 0.79 \text{ gm/min}$$



Glass Plate ($\theta = 24^\circ$) and a Water Surface



Glass Plate ($\theta = 47^\circ$) and a Water Surface



Glass Plate ($\theta = 90^\circ$) and a Water Surface

Figure 39. Photographs of Water Film Profiles Between Glass Plates and Water Surfaces.

The above capacity is proportional to average particle diameter, width of surface, and velocity of the surface. The calculations shown above apply only to that fraction of the feed that adhered to the disk. The total classification capacity of the entire system also contains those particles that did not impact the disk and those that rebounded from the disk since these mechanisms were also utilized for size classification. The total particle recovery efficiency for this system approaches 100 per cent as long as the feed rate and vacuum rates are adjusted to prevent any powder blow-out.

VI. CONCLUSIONS

The conclusions to be drawn from this study may be summarized as follows:

1. The size distribution of particles adhered to a solid surface shows a gradual but regular shift to smaller sizes as disruptive forces are increased.

2. The unusual rebounding trajectories of sub-sieve particles, the motion of which is subject to Stokes' law, may be utilized as a classifying mechanism.

3. An experimental classifier that operates on the two principles above has been designed and extensively evaluated. Excellent classification by particle size was achieved for materials having approximately spherical particles. Other materials consisting of irregular particles such as talc were also classified although generally not as well as particles which were more nearly spherical. The reasons for these differences are apparently due to the unpredictable rebounding characteristics of irregular particles and the much greater surface area present for adhesion with flat or elongated particles.

4. Good particle deagglomeration and dispersion are the prime requisites for successful classification by a rebounding and adhesion device. The "Wright Dust Feed Mechanism," manufactured by the L. Adams, Ltd.; Minerva Road, Chase Estate; London, England was found to be the most satisfactory device for producing a powder aerosol with predictable properties. A satisfactory feeding device for further deagglomeration at adequate feed velocities consisted of a section of 1/16 inch or 1/32 inch

stainless steel tubing with a slightly flared feed tip through which the aerosol was blown.

5. Brass, glass, plexiglass, and polished stainless steel were found to be the most suitable substrates, both from the standpoint of particle adhesion and substrate erosion. Other substrate materials such as paper or rubber were found to retain a large range of particle sizes very tenaciously, thus making it difficult to remove smaller particles selectively. Some preliminary experimentation is necessary with each powder to be classified in order to determine an optimum feed velocity for adequate adhesion as well as minimum substrate erosion and particle fracture.

6. The cross-section profile of liquid pools between particles and surfaces has been shown to be considerably more complicated than is normally assumed. Theoretical methods of calculation have been confirmed by near perfect agreement of experimentally and theoretically determined profiles. The modified mathematical models that have been proposed will permit more accurate calculations of adhesive forces due to liquid films. These models may also find use in particle sintering theory to describe better the driving forces for diffusion or evaporation due to curved surfaces.

7. Theoretical methods have been developed to predict quantitatively the effects of particle contact area and ambient air relative humidity on the forces of adhesion between particles and surfaces.

VII. RECOMMENDATIONS

Further studies should be made with a classifier of this design in low humidity environments so that the effects of particle charge and charge distribution can be examined. Recent studies by Ralston and others¹⁸ have demonstrated the feasibility of separation of mixed solids by an electrostatic device. A classifier of the type described in this report could be readily modified to incorporate also the features of an electrostatic separator with the possibility of achieving simultaneous separation of a mixed powder both by size and composition. Detailed studies of particle-surface interactions in the presence of significant electrostatic charge should also be examined.

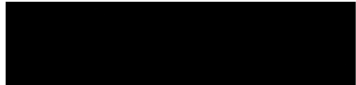
Studies should be made to confirm or reject theories advanced regarding the effects of particle contact area and relative humidity on adhesive forces. Ambient air relative humidity and particle contact area are interrelated influences that are of importance in many studies of small particle adhesion. The nature of their influence is not now clear due to contradictory reports in the literature. In this regard, studies should also be made to elucidate the effects of particle residence time on a surface and film diffusion rates on the forces of adhesion.

A study should be made to further develop analytical techniques for calculations of water film profiles. Further experimental studies should also be made of the three dimensional profiles between objects, e.g., a sphere and a water surface.


18. O. C. Ralston et al., Electrostatic Separation of Mixed Granular Solids, Elsevier Press (1961).

Finally, a prototype model classifier should be constructed utilizing the mechanism of adhesion and particle trajectory plus any other mechanisms that will enhance separation either by size or composition. Extensive testing of the design should be accomplished with many materials to assess any potential commercial value the device might have.

Respectfully submitted:


Clyde Orr, Jr. ✓
Project Director

Approved:


Frederick Bellinger, Chief
Chemical Sciences and Materials Division

VIII. APPENDIX

$$R \left[1 - \sqrt{1 - (\tilde{R})^2} \right] = r \left[1 - \sqrt{1 - (\bar{R})^2} \right]$$